FLOW CAMBRIDGE UNIVERSITY PRESS

TUTORIAL REVIEW

Laboratory generation of zero-mean-flow homogeneous isotropic turbulence: non-grid approaches

Arefe Ghazi Nezami[1],* 🆔, Margaret Byron[2] 🆔 and Blair A. Johnson[1] 🆔

[1]Department of Civil, Architectural and Environmental Engineering, University of Texas at Austin, Austin, TX 78712, USA
[2]Department of Mechanical Engineering, Penn State University, University Park, PA 16802, USA
*Corresponding author. E-mail: aghazinezami@utexas.edu

Abstract

Over the years, many facilities have been developed to study turbulent flow in the laboratory. Homogeneous isotropic turbulence (HIT) with zero mean flow provides a unique environment for investigating fundamental aspects and specific applications of turbulent flow. We provide an extensive overview of laboratory facilities that generate incompressible zero-mean-flow HIT using different types of actuators and configurations. Reviewed facilities cover a variety of geometries and sizes, as well as forcing style (e.g. symmetric versus asymmetric and unsteady versus steady). We divide facilities into four categories, highlighting links between their geometries and the statistics of the flows they generate. We then compare published data to uncover similarities and differences among various turbulence-generation mechanisms. We also compare the decay of turbulence in zero-mean-flow facilities with that observed in wind and water tunnels, and we analyse the connections between flow characteristics and physical aspects of the facilities. Our results emphasize the importance of considering facility geometry and size together with the strength and type of actuators when studying zero-mean-flow HIT. Overall, we provide insight into how to optimally design and build laboratory facilities that generate zero-mean-flow HIT.

Impact Statement

Ongoing development of experimental turbulence facilities enables the study of fascinating fluid dynamics phenomena and aids in the understanding of fundamental transport mechanisms. Generating zero-mean-flow homogeneous isotropic turbulence (HIT) in the laboratory is challenging and requires careful tuning of the experimental set-up. Each facility designed to produce HIT incorporates distinct features. This review summarizes the design and operation of several types of laboratory facilities that generate incompressible zero-mean-flow HIT, and provides a new meta-analysis relating facility size and energy injection methods to resulting turbulence properties across facility types. Understanding the capabilities and limitations of such facilities is also useful for those who use numerical simulations to understand complex fluid phenomena – both for validation of numerics and for planning and executing collaborations with experimentalists. With this compiled information as a resource, researchers can design well-tuned turbulence facilities that enable new advances in experimental fluid dynamics.

1. Introduction

Turbulence is important in environmental and industrial flows due to its impact on processes such as mixing, sediment transport and air–water interaction. Turbulence influences circulation in the ocean and the atmosphere, enhances the effective diffusivity of substances in the environment, drives sediment morphology and affects the health and survival of many living creatures. Numerical, laboratory and field studies have contributed to our understanding of turbulent flow. However, the stochastic nature of turbulence presents a unique challenge to repeatability and cross-comparison between flows (Pope 2000).

Laboratory studies provide a systematic way to isolate particular phenomena that may be more challenging to pursue via field studies or numerical simulations. Field conditions are difficult to control, due to the complexity of interactions between various drivers of flow. This can impede parametric exploration of desired variables. Numerical simulations, while rapidly increasing in capability, are still constrained by computational cost and challenges regarding imposing appropriate boundary conditions. Even laboratory-generated turbulence can be challenging to compare from one facility to another. It is therefore of interest to experimentally generate turbulence that is as free as possible from the signature of boundaries and forcing mechanisms, so that fundamental processes can be investigated across different facilities.

In most environmentally or industrially relevant flows, turbulence is neither homogeneous (statistically independent of spatial position) nor isotropic (statistically independent of orientation). Differences in boundary conditions or driving forces can dramatically change the characteristics of the resulting flow. However, the study of homogeneous and isotropic turbulence (HIT) can serve as a crucial starting point for improving our understanding of the energetics and transport potential of such flows, allowing us to simplify and generalize conclusions to yield more fundamental insight, and assess long-standing fundamental hypotheses in turbulence, such as Kolmogorov's hypothesis (Batchelor 1953; Lawson *et al.* 2019; Marston & Tobias 2022). Many specialized laboratory facilities have been developed to accomplish this. In this review, we discuss the history of HIT generation, presently existing facilities and their operation, challenges and opportunities presented by various approaches and overall best practices for generating HIT in the laboratory.

1.1. History of laboratory-generated HIT

1.1.1. Wind and water tunnels

The first purpose-designed HIT-generating facilities were wind (Simmons & Salter 1934; Comte-Bellot & Corrsin 1966) and water (Gibson & Schwarz 1963) tunnels. These facilities used a static, passive grid located upstream of the test section, causing HIT to develop downstream due to the interaction of wakes behind the grid. Makita (1991) introduced the 'active grid', in which protruding wings rotate at intervals to randomly block portions of the grid. This approach generated turbulence at a higher Reynolds number as compared with a passive grid. A review of active grids was recently published by Mydlarski (2017); both passive and active grids are used in modern facilities.

Uzkan & Reynolds (1967) modified passive-grid water tunnels to study mean-shear-free turbulence. They used a mobile bed, moving at the same speed as the streamwise velocity, to eliminate the mean velocity gradient (i.e. mean shear) at the bed. Similar experiments by Thomas & Hancock (1977) and Aronson, Johansson & Löfdahl (1997) generated high-Reynolds-number mean-shear-free turbulence via a passive grid in a wind tunnel, eliminating the mean boundary-layer-generated velocity gradient by moving the bed at the mean velocity of the flow. These mean-shear-free tunnel studies highlighted the underlying effects of boundaries in isolation of any mean velocity gradient; they were later used for validation and development of theories regarding the fundamental role of turbulence near boundaries (Hunt & Graham 1978; Biringen & Reynolds 1981; Hunt 1984; Perot & Moin 1995; Walker, Leighton & Garza-Rios 1996).

While eliminating mean shear gives insight into fundamental processes of turbulence, there is also value in removing mean flow. By removing mean flow, the complexities and uncertainties that arise in both natural and industrial environments are significantly reduced, offering a unique opportunity to isolate and investigate the physical driving mechanisms related to turbulent flow. For the study of multiphase flows, for example, zero-mean-flow turbulence can increase the feasible observation time of suspended bubbles, drops and particles, enabling Lagrangian analysis (Toschi & Bodenschatz 2009). In recent years, several turbulence facilities have been developed to generate HIT while minimizing the mean (background) flow or presence of recirculating currents. These facilities typically apply forcing via grids, fans, jets, loudspeakers or other point-source agitators.

1.1.2. Grid-stirred tanks

Rouse & Dodu (1955) developed the grid-stirred tank (GST), intended to generate HIT with neither recirculation nor mean shear via a planar grid oscillating along an axis normal to the grid plane. As the grid reciprocates linearly, its successive wakes interact to create HIT. Because of their simple design, low cost and relative ease of use, GSTs have remained popular for generating HIT in laboratories and are still in use today (e.g. Thompson & Turner 1975; Brumley & Jirka 1987; McCorquodale & Munro 2018). Properties of GST-generated turbulence depend strongly on grid characteristics, such as solidity (percent open area), rod/bar diameter and oscillation frequency (e.g. Thompson & Turner 1975; Hopfinger & Toly 1976; McDougall 1979; Nokes 1988). The distance from the grid to the homogeneous and isotropic region is also a function of the grid geometry; Hopfinger & Toly (1976) and Thompson & Turner (1975) determined that the developed isotropic region starts at a distance twice the mesh size (rod-to-rod spacing) away from the grid. This distance allows the wakes generated by the oscillating grids to decay and expand, ultimately interacting to generate HIT (Dohan & Sutherland 2002).

Grid-stirred tanks have frequently been used to investigate the effects of turbulence on environmental phenomena, including heat and mass flux across density interfaces (Thompson & Turner 1975; Hopfinger & Toly 1976; Xuequan & Hopfinger 1986; Nokes 1988; Kit, Strang & Fernando 1997; Holzner *et al.* 2006), gas transfer across a free surface (Jirka 2008), sediment transport and resuspension (Tsai & Lick 1986; Medina, Sánchez & Redondo 2001; Orlins & Gulliver 2003), flocculation (Casson & Lawler 1990; Cuthbertson, Dong & Davies 2010), flow through vegetation (Pujol *et al.* 2010), particle-laden flow (Ni *et al.* 2015) and many more. However, these facilities have some limitations. While intended to eliminate mean flow, GSTs have consistently been shown to exhibit overturning mean circulations and secondary flows at or above the scale of the turbulent fluctuations, a result of mass conservation (Cromwell 1960; Srdic, Fernando & Montenegro 1996; Mann, Ott & Andersen 1999; Dohan & Sutherland 2002; McKenna & McGillis 2004). In other words, secondary flows are inherent to GSTs due to the uniform planar forcing combined with the presence of relatively nearby boundaries. Reproducing a specific flow in these facilities is also challenging, since the generated flow is highly dependent on the initial condition and location of the grid (Xuequan & Hopfinger 1986; McKenna & McGillis 2004).

Several modifications have improved the performance of GSTs. Placing two parallel grids at opposite ends of the tank instead of using only one oscillating grid was found to improve isotropy and reduce the rate of decay (Villermaux, Sixou & Gagne 1995; Shy, Jang & Tang 1996; Srdic *et al.* 1996; Shy, Tang & Fann 1997; Yang & Shy 2003; Zellouf, Dupont & Peerhossaini 2005). Near the grids, the wakes generated are similar to those observed in single-grid facilities (Shy *et al.* 1996); however, the symmetric forcing generates HIT in the central region with a smaller decay rate compared with single-grid facilities (Zellouf *et al.* 2005). The use of two grids also provides the opportunity to agitate both layers in a two-layer fluid system (Mcgrath, Fernando & Hunt 1997). Li *et al.* (2020) used two pairs of parallel grids (i.e. four grids in total oscillating along a common axis) to enhance the fluctuating velocity in the direction of oscillation and reduce flow inertia normal to the oscillation axis, therefore mimicking a turbulent channel flow while maintaining minimal background flow. Some experiments used five or six oscillating grids in a single tank (Casson & Lawler 1990; Brunk 1996); Dickinson & Long (1983) placed a small tank inside of a larger tank with one oscillating grid located in the larger tank to reduce recirculations. Even though the use of multiple grids has decreased these recirculations, the dependence

of turbulence characteristics on large-scale motions in GSTs (Blum *et al.* 2010) led to a need to further decrease mean flow.

1.1.3. Synthetic jets and pointwise energy injection

While GSTs have achieved acceptable levels of homogeneity and isotropy for some applications, each grid still imparts momentum primarily in the grid-normal direction. This can lead to unavoidable anisotropy and to large-scale secondary (background) flows. As an alternative, pointwise energy injection, for example via synthetic jets, can reduce mean background flow and subsequent mean shear. Synthetic jets introduce momentum without a concomitant mass flux (Smith & Glezer 1998; Glezer & Amitay 2002), and can include fans, loudspeakers, propellers and bilge pumps. These actuators can be placed at the corners and/or along the walls of experimental facilities. The induced flows subsequently interact to form a central HIT region with small mean flow. Recent innovative techniques have also been developed to generate turbulence in laboratories via injection of vortex rings and magnetic particles (Gorce & Falcon 2022; Matsuzawa *et al.* 2023). We note that some facilities use rotating elements (e.g. counter- or co-rotating disks) to generate a swirling flow in the tank with a relatively small region of negligible mean flow (e.g. Douady, Couder & Brachet 1991; Fauve, Laroche & Castaing 1993; Voth *et al.* 2002; Ouellette *et al.* 2006; Klein *et al.* 2012; Webster & Young 2015; Ye, Manning & Hsu 2020). These facilities, sometimes called 'French washing machines', or 'von Kármán swirling tanks', reproduce important elements of turbulence but typically have strong mean flow outside of this small central region; therefore, they are not the focus of the present discussion. Other studies have used rotating elements such as grids and disks (with and without random forcing) to generate non-swirling, zero-mean-flow HIT (Liu, Katz & Meneveau 1999; Bordoloi, Verhille & Variano 2019; Pujara *et al.* 2021). Random forcing, coupled with the use of many rotating objects, reduces the strongly persistent vorticity that is otherwise characteristic of rotating-element-driven flow.

Synthetic jets are often used in planar arrays, which are more compatible with standard rectangular tanks than corner-mounted approaches (which typically require highly customized tank geometry). This creates momentum flux normal to the plane, as oscillating grids do; however, the jets are typically driven in a spatiotemporally varying pattern, unlike an oscillating grid. Random jet arrays (RJAs), introduced by Variano, Bodenschatz & Cowen (2004), are capable of generating HIT with high Reynolds number and negligible mean flow or boundary shear. Mean flows in facilities using RJAs (e.g. Variano & Cowen 2008; Pérez-Alvarado, Mydlarski & Gaskin 2016; Johnson & Cowen 2018) are among the lowest reported relative to alternative turbulence-generation mechanisms. In a RJA, synthetic jets are organized within a Cartesian-grid array, and they are randomly turned on and off according to specified forcing parameters. This stochasticity prevents the formation of persistent mean recirculation. The choice of a single or multiple array implementation, along with opportunities to tune the algorithm parameters, gives ample flexibility to optimize turbulence generation for a given application.

Here we have provided a brief overview of the historical development of incompressible zero-mean-flow HIT facilities. In the following sections, we explore these facilities in detail, focusing on the dynamic forcing mechanisms that came into use after the development of GSTs. In § 1.2, we provide a brief primer on the turbulent flow characteristics considered throughout the referenced studies to ensure consistent definitions and notation. In § 2, we explore the various flow-producing devices (i.e. fans, loudspeakers, jets and rotating elements) used in existing HIT facilities. Section 3 is devoted to synthesis and commentary on the characteristics of turbulent flow generation across different types of facilities. Finally, § 4 provides an overall summary of the present state of laboratory-generated zero-mean-flow HIT, as well as some guidelines for those seeking to construct new facilities.

1.2. Turbulence characteristics

To compare the performance of turbulence-generating facilities, we first define the parameters typically used to quantify turbulent flow. To establish notational consistency, here we present definitions for

the most common parameters used across the included studies (and further note that this list is non-exhaustive). In table 1, bold text represents vector quantities. The subscripts i, j and k can take on values corresponding to any of the three Cartesian coordinate directions.

In many of the facilities discussed below, symmetry is used to justify calculating parameters with two-dimensional flow data (e.g. u and w instead of u, v and w). For instance, in cases of planar forcing via a single jet array in the x–y plane, radial symmetry applies and k can be calculated as $k = \frac{1}{2}(2u'^2 + w'^2)$. Similarly, the direct calculation of ϵ can be simplified from nine velocity gradients to four given assumptions of continuity, symmetry and isotropy (Doron *et al.* 2001; Johnson & Cowen 2018). While we present isotropy as the ratio of RMS velocities (as in table 1), we note that isotropy can also be quantified via the ratio of integral length scales, where $\mathcal{L}_L / \mathcal{L}_T = 2$ indicates isotropy. These two ratios have sometimes indicated different degrees of isotropy (e.g. Carter & Coletti 2017; Johnson & Cowen 2018). Here we use Ω_{ij} because it is most commonly reported among the reviewed literature. We further emphasize that there are multiple methods for measuring the degree of isotropy of a given flow, but there is no standard test or threshold for declaring a particular flow to be isotropic or anisotropic. Parameters such as Ω_{ij} are helpful in that they assist in comparing facilities.

2. Actuator-based turbulence-generation mechanisms

In this section, we consider four types of forcing mechanisms (actuators) in order to explore their influence on flow generation and turbulence characteristics: fans, loudspeakers, jets and other rotating elements. Forcing may be steady, in which the actuators are active continuously, or unsteady, in which the actuators follow stochastic or deterministic time-varying patterns. Some actuators are better suited for only one working fluid (typically air and water), while others can be used in either gases or liquids. We compare how modifications to the operation and configuration of these actuators alter the resulting flow, and discuss practical drawbacks and advantages of each type of actuator. Most of the facilities discussed in this section, along with their turbulence characteristics, are presented in the Appendix (table 6).

2.1. Fan-driven turbulence generation

Homogeneous isotropic turbulence can be generated by placing several fans symmetrically about a central region, typically at the vertices of the facility, so that their momentum combines to generate HIT. The number of fans can vary, with a minimum number of four among the surveyed facilities. The rotational speed of the fans is typically kept constant during a single experiment (steady forcing). However, stochastic forcing can also be incorporated to modify the flow statistics and dependence on the forcing mechanism, as was recently done in a planar impeller array (Lawson & Ganapathisubramani 2022). Fan-driven facilities have been used to investigate the effects of turbulence on combustion (Semenov 1965; Andrews, Bradley & Lwakabamba 1975; Fansler & Groff 1990; Xu *et al.* 2017), preferential particle concentration in microgravity (Fallon & Rogers 2002), particle clustering (Salazar *et al.* 2008; Fiabane *et al.* 2012, 2013) and vaporization of chemicals and water droplets (Birouk *et al.* 1996; Birouk & Gökalp 2002; Li, Lohse & Huisman 2023). Table 2 summarizes some properties of fan-driven facilities that generate HIT with a negligible mean flow. Such facilities are usually small (<1 m) in size, with a symmetric forcing geometry. An example of fan-driven facility with a possible fan structure is shown in figure 1.

2.1.1. Fan configurations

Fan structural properties (e.g. number of blades, blade pitch angle (θ), fan diameter) and rotational speed can have strong effects on the generated turbulent flow (e.g. Kwon *et al.* 1992; Gillespie *et al.* 2000; Kumaresan & Joshi 2006; Ravi *et al.* 2013). According to Ravi *et al.* (2013), increasing the blade pitch angle and number of blades decreases turbulent Reynolds number, integral length scale, isotropy and homogeneity, but increases overall turbulent kinetic energy in the HIT region. The dissipation rate was unaffected by the number of blades, but it increased substantially when the pitch angle increased.

**Table 1.** *For caption see next page.*

Parameter	Description
Instantaneous velocity $U = (U, V, W)$	U, V and W describe the spatiotemporally varying velocity components in the x, y and z directions, respectively.
Mean velocity $\langle U \rangle \equiv \dfrac{1}{T} \displaystyle\int_0^T U \, dt$ $\overline{U} \equiv \dfrac{1}{\Psi} \displaystyle\int_0^\Psi U \, d\Psi$	$\langle U \rangle$ denotes time-averaged velocity over a duration T, frequently used as a proxy for ensemble averaging; $\overline{U}$ denotes spatially averaged velocity over a volume Ψ.
Instantaneous fluctuating velocities $u = (u, v, w) \equiv U - \langle U \rangle$	u, v and w are the spatiotemporally varying fluctuating velocity components, calculated via Reynolds decomposition to separate the fluctuating velocities from the ensemble-averaged velocities.
Root mean square (RMS) $u' = (u', v', w')$ $u_i' \equiv \sqrt{\langle u_i'^2 \rangle}$	u', v' and w' are the ensemble-average magnitude of the velocity fluctuations in the x, y and z directions, respectively.
Turbulent kinetic energy $k \equiv \dfrac{1}{2} \langle u \cdot u \rangle$	k is the amount of energy per unit mass associated with the turbulent velocity fluctuations. Based on k, a turbulent velocity can be defined as $u_T = \left(\dfrac{2}{3} k\right)^{1/2}$. In some studies, alternative turbulent velocity scales have also been defined.
Mean flow factor $M_i \equiv \dfrac{\langle U_i \rangle}{u_i'}$ $M^* \equiv \dfrac{\langle U \cdot U \rangle}{\langle u \cdot u \rangle}$	M_i is the ratio of the mean velocity to the RMS velocity in a given direction; M^* is the ratio of mean kinetic energy to turbulent kinetic energy; $M^* < 5\%$ has been found as a threshold for which mean flows can be neglected (Variano & Cowen 2008).

Table 1. *Common turbulent flow parameters used throughout the review. All definitions are taken from* Pope (2000) *and* Tennekes & Lumley (1972).

Parameter	Description
Integral length scale $\mathcal{L}_{ij}(\boldsymbol{x}, t) \equiv \dfrac{1}{R_{ii}(0, t)} \displaystyle\int_0^\infty R_{ii}(r_j, t)\, \mathrm{d}r$	L_{ij} represents the average size of an eddy; $R_{ii}(r, \boldsymbol{x}, t) \equiv \langle u_i(x + r_j, t) u_i(x, t) \rangle$ is the spatial autocovariance function and r_j is the separation in the j direction. Length scale $\mathcal{L}_{ij}$ is one representation of the average eddy size in a turbulent flow. When $i = j$, $\mathcal{L}_L = \mathcal{L}_{ii}$ is the longitudinal integral length scale; when $i \neq j$, $\mathcal{L}_T = \mathcal{L}_{ij}$ is the transverse integral length scale.
Large eddy length scale $\mathcal{L} = \dfrac{k^{3/2}}{\epsilon}$	$\mathcal{L}$ is of the same order as $\mathcal{L}_{ij}$ and is calculated via a scaling argument; it is representative of the large-scale eddies, and is generally not equal to $\mathcal{L}_L$.
Dissipation rate Direct method: $\epsilon = 2\nu \langle s_{ij} s_{ij} \rangle$ Scaling argument: $\epsilon = A \dfrac{u_T^3}{\mathcal{L}_L}$	ϵ is the rate at which energy is passed from larger to smaller scales, and can be calculated via several methods. In the direct method, $s_{ij} = \dfrac{1}{2}\left(\dfrac{\partial u_i}{\partial x_j} + \dfrac{\partial u_j}{\partial x_i}\right)$ is the strain rate and ν is the fluid kinematic viscosity. Using a scaling argument, A is an empirical constant (Sreenivasan 1984; Zhou 2021).
Kolmogorov scales Length: $\eta \equiv \left(\dfrac{\nu^3}{\epsilon}\right)^{1/4}$ Time: $\tau_\eta \equiv \left(\dfrac{\nu}{\epsilon}\right)^{1/2}$	The Kolmogorov scales demarcate the end of the inertial range; motions smaller than these will be dissipated by viscosity.
Reynolds number $Re_\lambda = \dfrac{u_T \lambda}{\nu}$ $Re_T = \dfrac{u_T \mathcal{L}_L}{\nu}$	Re quantifies the ratio of inertia to viscosity in a flow, as well as scale separation between large and small eddies. For the work reviewed here, Re_λ is most commonly reported (where λ is the Taylor microscale, an intermediate length scale of the flow). Parameter Re_T is the turbulent Reynolds number. Note that different studies use various definitions of Re_λ and Re_T.
Isotropy ratio $\Omega_{ij} \equiv \dfrac{u_i'}{u_j'}$	Ω indicates the level of isotropy between two given directions.

Table 2. *Characteristics and flow statistics of fan-driven turbulence facilities, where f is rotational fan speed and other variables are defined in § 1.2. Parameter D_{fan} is the diameter of the fan. Note that throughout the following sections, $\mathcal{L}$ is shown with * and $\mathcal{L}_L$ is shown with $^+$. The superscript $^\times$ indicates values estimated by the authors from provided data. Note that in the study of Ravi, Peltier & Petersen (2013) multiple fan configurations were used; the result shown is for the baseline fan prototype.*

Authors	f (r.p.m.)	No. of fans	Blade length (cm)	D_{fan} (cm)	k (cm² s⁻²)	Re_λ	$\mathcal{L}_L, \mathcal{L}$ (cm)	Facility dimensions (m)	Facility geometry
Fallon & Rogers (2002)	—	8	—	5.08	$13.5^\times$	50	$15^{\times *}$	$L = 0.3$	Cubic
Birouk, Sarh & Gökalp (2003)	650–2700	8	—	11	$1–14.5 \times 10^3$	45–92	0.86^+	$L = 0.4$	Cubic
de Jong et al. (2009)	1900–3900	8	—	—	$1.91–17.2 \times 10^3$	104–184	$5.53–6.02^+$	$L = 0.4$	Cubic
Zimmermann et al. (2010)	60–560	12	—	10	$3.34–238.1^\times$	150–330	$6–10^*$	$L = 0.4$	Icosahedron
Ravi et al. (2013)	8300	4	3.8	7.62	3.3×10^4	277	5.4^*	$D = 0.305$ $H = 0.356$	Cylinder
Dou et al. (2016)	1500–3500	20	—	16	$0.73–3.65$	246–384	$16–18^*$	$L = 0.2$	Truncated icosahedron
Bradley, Lawes & Morsy (2019)	1000–6000	4	7.5	—	$2.16–77.76 \times 10^{4 \times}$	220–555	$1.91–2.15^+$	$D = 0.38$	Sphere
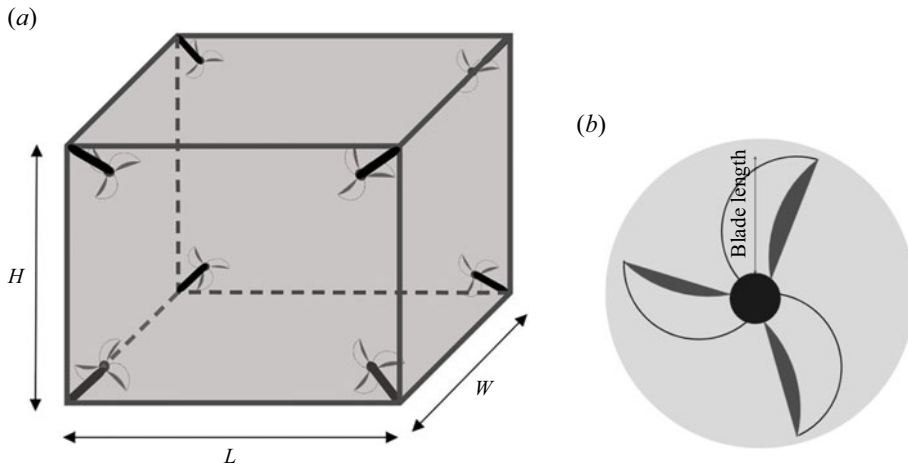
Figure 1. *(a) Schematic of a cuboidal fan facility with height H, width W and length L. (b) Schematic of a fan with three blades.*

This may be due to stronger axial momentum input at higher pitch angles, which leads to a decrease in both isotropy and homogeneity in the central volume. Their results show that changing the rotational frequency in fan-driven facilities does not affect the value of $\mathcal{L}_L$.

In fan-generated HIT, the magnitudes of the fluctuating velocities can be increased by increasing the rotational frequency (f) of the fans. Dou *et al.* (2016) proposed that turbulence strength (similar to u_T; see table 1) is linearly correlated with f, and Re_λ is proportional to the square root of fan speed. Similarly, Birouk *et al.* (2003), Zimmermann *et al.* (2010) and Bradley *et al.* (2019) detected a linear relationship between the turbulent fluctuating velocities and f (figure 2), albeit with slightly different slopes. This linear relationship between u' and f implies that the fluctuating velocities scale with the tip speed of the fan, although the precise scaling likely depends on the facility and fan geometry. However, changing f did not modify the integral length scales (Gillespie *et al.* 2000; Bradley *et al.* 2019). The overall geometry of fan-driven facilities is more influential on $\mathcal{L}_L$ than either the fan structure or rotational speed, as we discuss in § 3.3. Leisenheimer & Leuckel (1996) explored the effects of vessel size, number of fans and fan diameter on the generated HIT. They concluded that the vessel size was the main contributor to the value of the integral length scale, and proposed a linear relationship between $\mathcal{L}_L$ and the radius of the facility.

Bradley *et al.* (2019) found that while $\mathcal{L}_L$ remains constant with increasing fan speed, integral time scale, τ, a characteristic eddy turnover time scale, decreases while RMS velocity increases. This can be understood via a dimensional argument: at large length scales, viscosity is not important, so the forcing frequency provides the only inherent time scale of $1/f$. Thus, for a given fan structure, τ decreases as f increases while $\mathcal{L}_L$ remains constant (since the inherent length scales of fan diameter, facility size and fan spacing do not change with f). Increasing f produced a smaller region of HIT, and altered the normality of the distribution of the fluctuating velocities (Ravi *et al.* 2013; Bradley *et al.* 2019) (figure 2). Bradley *et al.* (2019) observed that the largest, most homogeneous and most isotropic region of HIT in their studies occurred when f was set to a value between 2000 and 4000 r.p.m. (similar to Birouk *et al.* (2003)).

2.1.2. Advantages and drawbacks

Since the HIT region is generated as a result of the interactions between local vortical flows induced by each fan, its characteristics and RMS velocities vary with respect to these local motions and fan structures. One advantage of these facilities is that an increase in the magnitude of the fluctuating velocities does not necessarily correspond to an increase in the background mean flow. The mean flow is negligible in most studies presented in this section, and the volume of the HIT region is fairly small
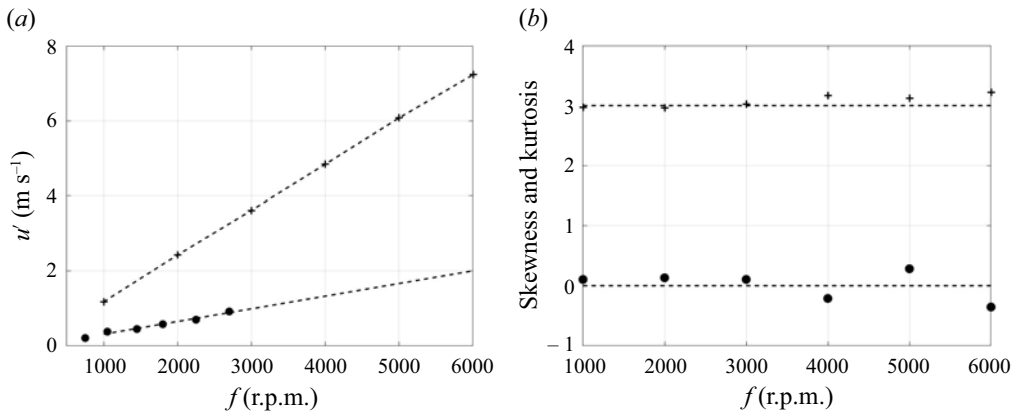
Figure 2. *(a) Changes to u′ with respect to the fan speed, using data from Birouk et al. (2003) (●) and Bradley et al. (2019) (+). (b) Values of skewness (●) and kurtosis (+) of u′ with a Gaussian-fitted distribution when changing fan speed, using data from Bradley et al. (2019).*

(less than approximately 10 % of the facility size, as determined from measurements such as planar particle image velocimetry). In fan-driven facilities, an increase in the magnitude of the RMS velocities does not necessarily correspond to an increase in the mean velocity. Therefore, although the HIT region is small, the mean flow within that region remains negligible. Another advantage of this type of facility is that the time required for the flow to reach steady state from initiation of fan motion is small (e.g. 10 s for Dou *et al.* (2016)), because the values of τ in these facilities are relatively small (e.g. <20 ms for Bradley *et al.* (2019)). In general, the turbulent flow characteristics are relatively consistent across all of the fan facilities presented here. Flows generated via fans are highly reproducible and do not depend significantly on initial conditions.

2.2. Loudspeaker-forced turbulence

Acoustic actuators, such as loudspeakers, have been used as synthetic jets to generate HIT. As with fan-driven facilities, the actuators are mounted symmetrically around a central region in which HIT is created. In each loudspeaker a diaphragm of diameter d_L placed in a cavity vibrates sinusoidally with frequency F and a specific phase, which can be deterministic (constant frequency and phase) or stochastic (variable frequency within an experiment). In front of the cavity, various orifices (usually circular with a specific diameter $d_J < d_L$) are placed to produce jet-like motion via mass conservation within the cavity. The frequency and phase of the inputs are tuned to diminish the generation of secondary flows or standing waves in the tank, as well as to reduce return flows that form due to mass conservation within the larger chamber when the apparatus is closed (Lu *et al.* 2008; Sabban & van Hout 2011; Hoffman & Eaton 2021). As introduced in § 1.1.3, stochastic forcing diminishes mean flow by disrupting large-scale recirculation. In unbounded, open-air facilities (e.g. that of Goepfert *et al.* 2010), stochastic forcing is not needed to avoid mean flow (see § 3.2 and figure 3). Loudspeaker-driven HIT with zero mean flow has been used to study phenomena including pollen dispersal in turbulent air (Sabban & van Hout 2011), particle movements and trajectories (Sabban, Cohen & van Hout 2017), ice melting in turbulence (Stapountzis *et al.* 2015) and zooplankton in oceanic turbulence (Webster, Brathwaite & Yen 2004; DiBenedetto *et al.* 2022). Table 3 summarizes some properties of loudspeaker-driven facilities that generate zero-mean-flow HIT.

2.2.1. Loudspeaker characteristics
As with fan-driven facilities, loudspeaker-driven facilities can generate HIT with low mean flow; for example, Hwang & Eaton (2004) measured an HIT area of 4 cm × 4 cm via planar particle image
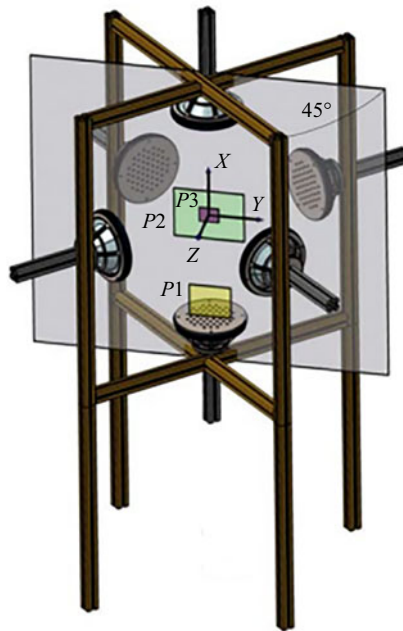
Figure 3. *Loudspeaker facility. Reproduced from Goepfert et al. (2010).*

velocimetry in their facility. To improve turbulence characteristics, various barriers may be placed in front of the loudspeakers. For example, Hwang & Eaton (2004) placed a mesh along the speaker faces to break down the large-scale fluid structures generated by the loudspeaker, thereby introducing intermediate length scales. Goepfert *et al.* (2010) and Webster *et al.* (2004) used plates with a lattice of smaller holes, which forced flow into higher-velocity jets. This structure provided a high outlet velocity and a uniform momentum flux without a significant pressure change.

Increasing the amplitude of the speakers directly affects the fluctuating velocity, dissipation rate and turbulent kinetic energy (Webster *et al.* 2004; Sabban & van Hout 2011; Hoffman & Eaton 2021). Webster *et al.* (2004) showed that increasing the amplitude of the input signal of the loudspeakers improved Ω and increased Re_λ. Sabban & van Hout (2011) observed the same behaviour, along with increased k and slightly decreased mean flow. Increasing speaker amplitude (and therefore Re_λ) leads the probability density function of the fluctuating velocities to fall closer to a Gaussian distribution. However, at a somewhat higher Reynolds number ($Re_\lambda > 165$), Hoffman & Eaton (2021) did not observe any significant changes in Ω or mean flow strength with increasing loudspeaker input power.

2.2.2. Advantages and drawbacks

As in fan-driven facilities, loudspeakers may be actuated individually to tune the generated flow and create intentional anisotropy. Some configurations allow for modification of the fluctuating velocities without changing the Reynolds number or the mean flow generated in the facility (e.g. Bewley, Chang & Bodenschatz 2012; Chang *et al.* 2012; Bewley, Saw & Bodenschatz 2013). Using a scaling argument, Hoffman & Eaton (2021) proposed that loudspeaker-driven facilities can be designed based on the desired Reynolds number and dissipation rate, providing a flexible platform to generate HIT. Similar to fan-driven facilities, the time to reach an equilibrium turbulent state in loudspeaker-driven turbulence is short (e.g. 60 s for Lu *et al.* (2008)).

On the downside, Hoffman & Eaton (2021) found it challenging to generate HIT with negligible mean flow. This is an indication of the importance of the physical characteristics of the chamber with respect to the generated turbulence (see § 3.3). Additionally, the homogeneous isotropic region is small, even when the facility is large; for example, the apparatus used by Bewley *et al.* (2012) exhibited a region of HIT of only 50 mm in diameter despite a facility inner diameter of 1 m.

Table 3. *Geometry and turbulence characteristics of loudspeaker-driven facilities. Parameter L_S indicates distance between the speakers for the unbounded facility of Goepfert et al. (2010). Note that in the study of Chang, Bewley & Bodenschatz (2012), multiple Ω with the same Re_λ were studied; here we only include results for the value of $\Omega \approx 1$. The remaining superscripts are explained in table 2.*

Authors	No. of loudspeakers	d_L (cm)	d_J (cm)	F (Hz)	Re_λ	$\mathcal{L}_L, \mathcal{L}$ (cm)	k (m^2 s^{-2})	Facility dimensions (m)	Facility geometry
Hwang & Eaton (2004)	8	1.9	4	90–110	220	5.6*	1.1	$L = 0.41$	Cubic
Webster et al. (2004)	8	2.54	0.32	30–40	10–68	3×*	0.15–1.27×	$L = 0.4$	Cubic
Lu et al. (2008)	8	—	—	—	260	15×*	0.54×	$L = 0.5$	Cubic
Goepfert et al. (2010)	6	21.5	0.6	42	237	3.6+	0.91	$L_S = 0.64$	Cubic/no boundaries
Sabban & van Hout (2011)	8	13	—	90–100	144–162	4.9–5.8×*	0.35–0.51×	$L = 0.4$	Cubic
Chang et al. (2012)[2]	32	16.5	5	50–3000	481	39×*	1.91	$D = 0.99$	Truncated icosahedron
Hoffman & Eaton (2021)	32	10	1.6	70–76	165–240	6.83–8.17*	0.14–0.81	$D = 0.64\ H = 1$	Cylindrical

2.3. *Turbulence generation via jet arrays*

Another mechanism for generating HIT with negligible mean flow, introduced by Variano *et al.* (2004), is the RJA. Jets, organized in a planar array at a distance S from one another, are stochastically turned on and off to generate HIT at some distance from the jet plane. Often, such arrays use submersible pumps that accelerate fluid effectively from a point (injecting only momentum, not mass, in keeping with the definition of a synthetic jet). In other instances, pressure opening valves are used to produce the momentum needed for HIT generation (Variano *et al.* 2004; Carter *et al.* 2016; Esteban, Shrimpton & Ganapathisubramani 2019; Masuk *et al.* 2019). In valve-based RJAs, the suction and ejection location are located apart from each other; thus, they may not be categorized as conventional synthetic jets. Non-synthetic jets may also be used (e.g. Krawczynski *et al.* 2006; Krawczynski, Renou & Danaila 2010), but they may not necessarily achieve zero-mean-flow HIT.

Random jet arrays have been used widely to investigate a variety of topics, such as bed morphology and sediment transport (Johnson & Cowen 2020), the effect of background flow on jets (Lavertu 2006; Khorsandi, Gaskin & Mydlarski 2013), the process of homogeneous electrodeposition in turbulence (Delbos *et al.* 2009), the kinematics of particles (Bellani *et al.* 2012; Meyer, Byron & Variano 2013; Byron *et al.* 2015; Pujara *et al.* 2018; Tinklenberg, Guala & Coletti 2023), the dissolution of large particles (Oehmke & Variano 2021), clustering of particles (Pratt, True & Crimaldi 2017; Petersen, Baker & Coletti 2019) and the melting of ice in turbulence (McCutchan 2020). Table 4 lists the known facilities that use RJAs for zero-mean-flow turbulence generation with their concomitant turbulence characteristics.

Flows in RJA-driven facilities may generally be divided into three regions, each with different turbulence characteristics. Immediately adjacent to the jet array, there is a jet-driven flow with high momentum flux in the array-normal direction due to the jet pulses and return flows. Some distance downstream is a jet merging region where the jets interact with each other and with the ambient (non-jet-driven) fluid. Axial momentum flux and mean flow are still high in this region. At some distance further downstream, there is a region of HIT with negligible mean flow in which the individual jet pulses are no longer distinguishable. If the HIT region is adjacent to an interface (e.g. solid wall, free surface, sediment bed, density stratification), then a boundary-affected region of flow may exist.

The RJAs are modular and can be configured to suit different experimental goals. In single-RJA facilities, the array of jets may fire vertically from the bottom (Variano & Cowen 2008) or top (Johnson & Cowen 2018) of a large tank, or placed so that the jets fire horizontally from one side (Delbos *et al.* 2009). Multiple RJAs can provide symmetric forcing by placing two arrays of jets at opposite sides of a rectangular tank (Bellani *et al.* 2012; Bellani & Variano 2014; Carter *et al.* 2016; Carter & Coletti 2017, 2018), or four arrays in an octagonal tank (Bang & Pujara 2023). This 'facing array implementation' (Bellani & Variano 2014) increases the size of the HIT region, improves Ω and helps to further break down tank-scale secondary flows. Alternatively, each jet can be placed individually at the vertices or along the facility edges to generate a set-up similar to that of fan-driven facilities (McCutchan & Johnson 2023). An example of a single RJA is shown in figure 4.
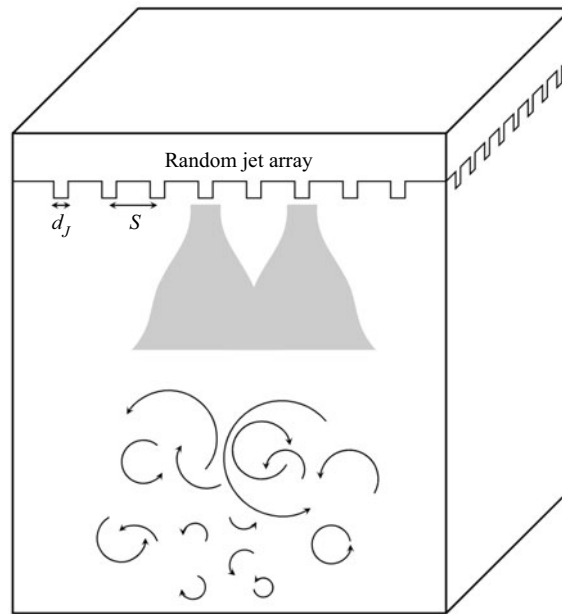
2.3.1. *Jet-driving algorithm*

Variano & Cowen (2008) were the first to employ the sunbathing algorithm to greatly reduce mean flows. In this algorithm, jets are randomly actuated in such a way as to interrupt the secondary circulation that would be present if all jets fired simultaneously or in a fixed pattern. The instantaneous time that each individual jet is on (T_{on}) or off (T_{off}) is sampled from a Gaussian distribution with predetermined mean μ and variance σ. After an initial transient period, the percentage of jets firing at any given time will statistically approach $\phi_{on} \equiv \mu_{on}/(\mu_{on} + \mu_{off})$. Most RJAs are controlled using this algorithm.

Several studies have explored how changing the jet-driving algorithm affects the turbulent flow generated in the facility (e.g. Variano & Cowen 2008; Carter *et al.* 2016; Pérez-Alvarado *et al.* 2016; Johnson & Cowen 2018). When compared with other algorithms, the sunbathing algorithm was found to generate the highest k, the lowest M^* and generally high degrees of isotropy (Variano & Cowen

Table 4. *Characteristics and flow statistics of jet-driven turbulence facilities. Parameter d_J is the pump outlet diameter and Re_J is the pump outlet Reynolds number, defined as $U_J d_J/\nu$, where U_J is the pump outlet velocity. In the study of* Pérez-Alvarado et al. (2016), Re_T *is presented instead of Re_λ. The superscript* [†] *indicates facilities that have two facing jet arrays. The remaining superscripts are explained in* table 2.

Authors	Re_J	d_J (mm)	S (cm)	Re_λ	No. of jets	k ($cm^2\,s^{-2}$)	$\mathcal{L}, \mathcal{L}_L$ (cm)	Facility dimension (m)
Variano et al. (2004)	4000	9	3.6	30–50	3×3	—	—	$L = 0.108$ $H = 0.4$
Variano & Cowen (2008)	14 000	21.9	10	314	8×8	27.7[×]	7.57[+]	$L = 0.8$ $H = 0.91$
Delbos et al. (2009)	7000	0.95	4.5	—	8×8	—	—	$L = 0.36$
Khorsandi et al. (2013)	20 000[×]	31.75	15	—	6×10	3.48[×]	11[+]	$L = 0.9$ $W = 1.5$ $H = 2.4$
Bellani & Variano (2014)	—	21.9	10	338	$2\text{–}8 \times 8$[†]	6.07	9.5[+]	$L = 0.8$ $H = 3.6$
Carter et al. (2016)	14 000	10	10	259–473	$2\text{–}8 \times 16$[†]	38.4–86.6[×]	9–14.6[+]	$L = 1.1$ $W = 2$ $H = 2.4$
Pérez-Alvarado et al. (2016)	20 000[×]	31.75	15	2360	6×10	6.31	11.5[+]	$L = 0.9$ $W = 1.5$ $H = 2.4$
Johnson & Cowen (2018)	22 000 28 000	21.98	10 5	288–378 197–262	8×8 16×16	32–51.5 37.5–68	6.8–9.71 4.52–5.19[+]	$L = 0.8$ $H = 1$
Esteban et al. (2019)	25 000[×]	18	13	587	$2\text{–}8 \times 6$[†]	38.5[×]	9.1[+]	$L = 0.85$ $W = 1$ $H = 2$

Figure 4. *Schematic of an RJA facility with downward-facing jets, in which d_J is the outlet jet diameter and S is the centre-to-centre spacing between adjacent jets.*

2008; Pérez-Alvarado *et al.* 2016). Variano & Cowen (2008) compared the sunbathing algorithm with a deterministic algorithm with the same ϕ_{on} and found a two to three times reduction of mean flows when using the sunbathing algorithm ($M^* < 5$).

Pérez-Alvarado *et al.* (2016) tested several additional algorithms, aiming to determine whether the spatial distribution of active jet forcing affected homogeneity and isotropy. For example, their 4SEC-TRANDOM algorithm divided the jet array into four quadrants, in which one 'master' quadrant was run according to the sunbathing algorithm and the rest were copied and reflected to preserve symmetry about the grid centre. Their CHESSBOARD algorithm turned 50 % of the jets on and the rest off at all times in a chessboard pattern; this pattern was compared with variants EQUALCHESS (which changed the on/off states every 12 s) and RANDOMCHESS, in which the chessboard pattern was preserved but on/off states were changed according to a Gaussian distribution as in the sunbathing algorithm. Among all tested algorithms, the sunbathing algorithm (with no spatial correlation of active jets) produced turbulence with the lowest mean flow strength and values of Ω closest to unity.

Altering the algorithm parameters can control turbulence statistics. For example, increasing T_{on} has been shown to increase k, L_L and Re_λ (Carter *et al.* 2016; Johnson & Cowen 2018, 2020). However, Variano & Cowen (2008) stated that increasing T_{on} beyond a certain value no longer increases the turbulence production, and the increase in RMS velocities is a result of the turbulence induced by the individual jet forcing. Variano & Cowen (2008) also found an optimum range for the value of ϕ_{on} that maximized k irrespective of further increases in T_{on}. Johnson & Cowen (2018) found that within this range, the particular value of ϕ_{on} has a negligible effect on the RMS velocities. The outlet jet velocity is another factor that can be modified to change the strength of the turbulence. Pratt *et al.* (2017) observed that increasing the input voltage of the pumps (which controls jet velocity and subsequently changes the jet outlet Reynolds number) increased Re_λ and the dissipation rate while λ remained nearly constant.

Johnson & Cowen (2018) showed that while changing T_{on} affected k and Re_λ, the turbulence remained horizontally homogeneous (i.e. statistically independent of position in x–y planes parallel to the orifice plane of the jet array) and nearly isotropic with no significant changes in the mean flow (for the ranges of T_{on} and ϕ_{on} considered). On the other hand, Carter & Coletti (2017) found a decrease in isotropy

with increased T_{on} (and correspondingly higher Re_λ). Carter et al. (2016) also argue that the degree of anisotropy in their results was inherent to their facility, similar to unavoidable anisotropy of an individual jet in the self-similar region (e.g. at a distance $>30d_J$) (Burattini, Antonia & Danaila 2005).

2.3.2. *Effect of RJA physical design*

The physical properties of jet-driven facilities can affect characteristics of the generated turbulent flow. Such properties include the facility size, jet spacing, jet diameter, pump outlet extensions and distance between arrays. The significance of the facility proportions is apparent in studies with the same set-up configuration (e.g. two facing arrays) and similar flow energetics (e.g. Re_λ), but with different tank sizes and different corresponding ratios (e.g. ratio of distance between the arrays and the jet spacing). For example, the turbulence in Bellani & Variano (2014) was isotropic, while the turbulence in the facilities used by Carter et al. (2016) and Esteban et al. (2019) was anisotropic. The effect of tank size can also be seen by looking at table 4, which shows that larger facilities tend to have greater values of the integral length scale. Generally, in many RJA facilities, the size of the HIT region expands beyond $\mathcal{L}_L$. However, we note that this is also true for other types of facilities (e.g. Zimmermann et al. 2010).

In addition to the size of the facility, ratios of the pump outlet diameter, spacing and distance from the arrays affect the turbulence statistics. For example, z_J/S, where z_J is the distance from the jet array and S is the jet-to-jet spacing, can be used as a parameter to characterize different regions in a RJA-driven flow. The data of Khorsandi et al. (2013) and Pérez-Alvarado et al. (2016) suggest that turbulence is still developing at $z_J/S > 5$. An increase in k, increase in the degree of isotropy and decrease in the mean flow strength can be seen beyond $z_J/S = 5$. Variano & Cowen (2008) proposed that z_J/S must be greater than 6 to achieve HIT with negligible mean flow. On the other hand, Masuk et al. (2019) explained that where the half-width of the jets exceeds the jet spacing, the jet flows interact and therefore produce HIT. Masuk et al. (2019) collected measurements at $z_J/d_J = 76$ to ensure well-developed flow. It should be noted that the region corresponding to $z_J > 6S$ may not coincide with the location at which the half-width of the jets is greater than the jet spacing across all jet-driven facilities.

In a two-facing-array set-up, the influence on the flow in response to changing the distance between the arrays and S was studied separately by Carter et al. (2016). The results showed that changing the value of S did not have any impact on the integral length scale, whereas decreasing the distance between the arrays led to a decrease in $\mathcal{L}_L$ for a given value of Re_λ. However, Ω was not affected by changing either spacing, as the turbulence remained anisotropic in all scenarios with an increase in Re_λ. In general, the development of the zero-mean-flow HIT region is constrained by the distance between the two arrays relative to the spacing between the jets in the array. This is particularly relevant for facilities with a single planar jet array, where the distance between the array and the opposing boundary (such as a solid boundary or free surface) plays an important role.

One additional method of modifying the flow development is to place a mesh immediately downstream of the jet outlets (Bellani & Variano 2014; Carter et al. 2016). Carter et al. (2016) observed that by placing a mesh in front of the jets, $\mathcal{L}_L$ and Re_λ decreased for the same algorithmic forcing. In some cases, $\mathcal{L}_L$ was reduced by approximately 30 % in response to the mesh. Inserting a mesh breaks down the eddies generated by the jets and thus creates broader and more uniform momentum immediately downstream of the array. Based on the data summarized in table 4, physical aspects related to the pumps such as outlet Reynolds number, pump outlet diameter or addition of a nozzle to the pump outlet do not correlate directly with the turbulence statistics. However, more studies are needed to investigate the effects of jet outlet properties on the statistics of the generated turbulence.

2.3.3. *Drawbacks and advantages*

One advantage of using RJAs is that the time to reach equilibrium in the statistics of the turbulent flow is very small. Variano & Cowen (2008) mentioned that after only 3 s, the flow can be considered statistically steady. Similarly, Carter et al. (2016) found most of the flow properties reached steady state after approximately 10 s. However, Esteban et al. (2019) stated this time to be 5 min, which is notably

longer compared with the other studies. Variano & Cowen (2008) mentioned that repeatability is readily achievable, particularly in contrast to GST facilities where the resultant flow is highly dependent on initial conditions (McDougall 1979; Dohan & Sutherland 2002).

Jet arrays can be placed in different locations, thus enabling simple facility modifications that can generate different flow environments to study a wide range of applications. Another advantage of this type of facility is that turbulent flow statistics can be controlled by changing the input algorithm for the same physical geometry and pump characteristics. Since ϕ_{on}, T_{on} and U_J can be independently modified, the input energy in these facilities can be adjusted to produce high-Reynolds-number turbulence. However, generation of isotropic turbulence has been more challenging in some RJA facilities (Carter *et al.* 2016; Bradley *et al.* 2019) due to the decay of turbulence. Since these facilities have a high degree of freedom due to the number of jets and the variability in the algorithm, care is needed to produce optimal flow characteristics.

2.4. *Rotating turbulence actuators*

One other type of facility for generating zero-mean-flow HIT uses rotating elements that induce momentum and vorticity. These rotating objects are either forced stochastically (e.g. Pujara *et al.* 2021) or spin with a constant rotational speed (e.g. Berg *et al.* 2006; Bounoua, Bouchet & Verhille 2018). Although the actuators rotate, similarly to the rotation of fans (recall § 2.1), the actuators in these facilities are categorized separately. Properties of fans are relatively well characterized and universal (Ravi *et al.* 2013); however, because the actuators used here consist of disks, grids or other devices, or because they are fans that are used unconventionally (i.e. they do not induce momentum towards the centre of the facility), they have been categorized separately. The facilities presented herein all have markedly different geometric configurations from one another. In general, most of the studies showcasing these facilities focus on specific applications rather than the properties of generated turbulence; therefore, the data presented here are limited to those reported by each study.

Liu *et al.* (1999) generated HIT by rotating four grids, such that adjacent grids had opposite rotational directions. This method generated turbulence with small mean flow that was shown to be homogeneous and isotropic, with no significant change in the profile of RMS velocities in any direction. Berg *et al.* (2006) used propellers mounted horizontally, rather than facing the centre of the facility; the rotational direction of each propeller changed at fixed intervals to generate zero-mean-flow HIT (figure 5c). Using disks with blades was another approach developed by Bounoua *et al.* (2018) and Bordoloi *et al.* (2019). Recently, Pujara *et al.* (2021) used four rotating panels and placed a mesh in front of the panels to study particle trajectories in zero-mean-flow HIT. In all of these facilities, the rotational speed of each rotating element was independent of the others. Table 5 summarizes the facilities using rotating objects along with measured turbulence statistics.

As with the other types of turbulence facilities, modifying the input momentum from the rotating elements can affect the resultant turbulence characteristics. For example, increasing the rotational frequency of these elements has been shown to increase the turbulent Reynolds number (Pujara *et al.* 2021). In the study of Pujara *et al.* (2021), increasing the rotation frequency of the panels resulted in a decrease of the mean flow strength, but isotropy was sacrificed. Also, Pujara *et al.* (2021) observed a slight decrease in L_L when increasing Re_λ. The variation between the facilities that use rotating actuators emphasizes that there is not a prescribed formula for designing a zero-mean-flow HIT facility. Each of the facilities incorporates design elements tested in prior facilities, though the implementations are unique. All of the facilities with rotating elements incorporated symmetric forcing configurations. As with other types of turbulence facilities, selection of the type and quantity of rotating elements, the presence or absence of a grid and independence in the rotation of each element all contribute to the generation of turbulence with distinct characteristics.

Table 5. *Characteristics and flow statistics of turbulence facilities with rotating elements. Parameter f_r indicates the rotational speed of the rotating element. Superscripts are explained in* table 2.

Authors	Rotating element and description	No. of rotating elements	f_r (r.p.m.)	Re_λ	k (cm² s⁻²)	$\mathcal{L}, \mathcal{L}_L$ (cm)	Facility dimension (m)	Facility geometry
Liu et al. (1999)	Rotating grids, in which each grid consists of two perpendicular grids with height 10 cm and width 8.8 cm, with 1 mm diameter rods spaced at 5 mm	4	3200	290	48.5$^\times$	9.1*	$L = 0.3$	Cubic
Berg et al. (2006)	Propellers	8	—	172	5.96$^\times$	4.8$^+$	$L = 0.32$ $H = 0.5$	Cuboid
Bounoua et al. (2018)	Disks with diameter 17 cm with mounted straight blades of height 5 cm	8	300–900	350–610	—	—	$L = 0.6$	Cubic
Pujara et al. (2021)	Paddles comprised of rigid mesh with square openings 2× 2 mm²; in front of each pair of paddles a screen is placed with 58 % open area and holes of diameter 5 mm	4	—	64–142	0.67–8.07	2.52–2.2$^+$	$L = 0.0625$ $W = 0.0825$ $H = 0.1225$	Cuboid
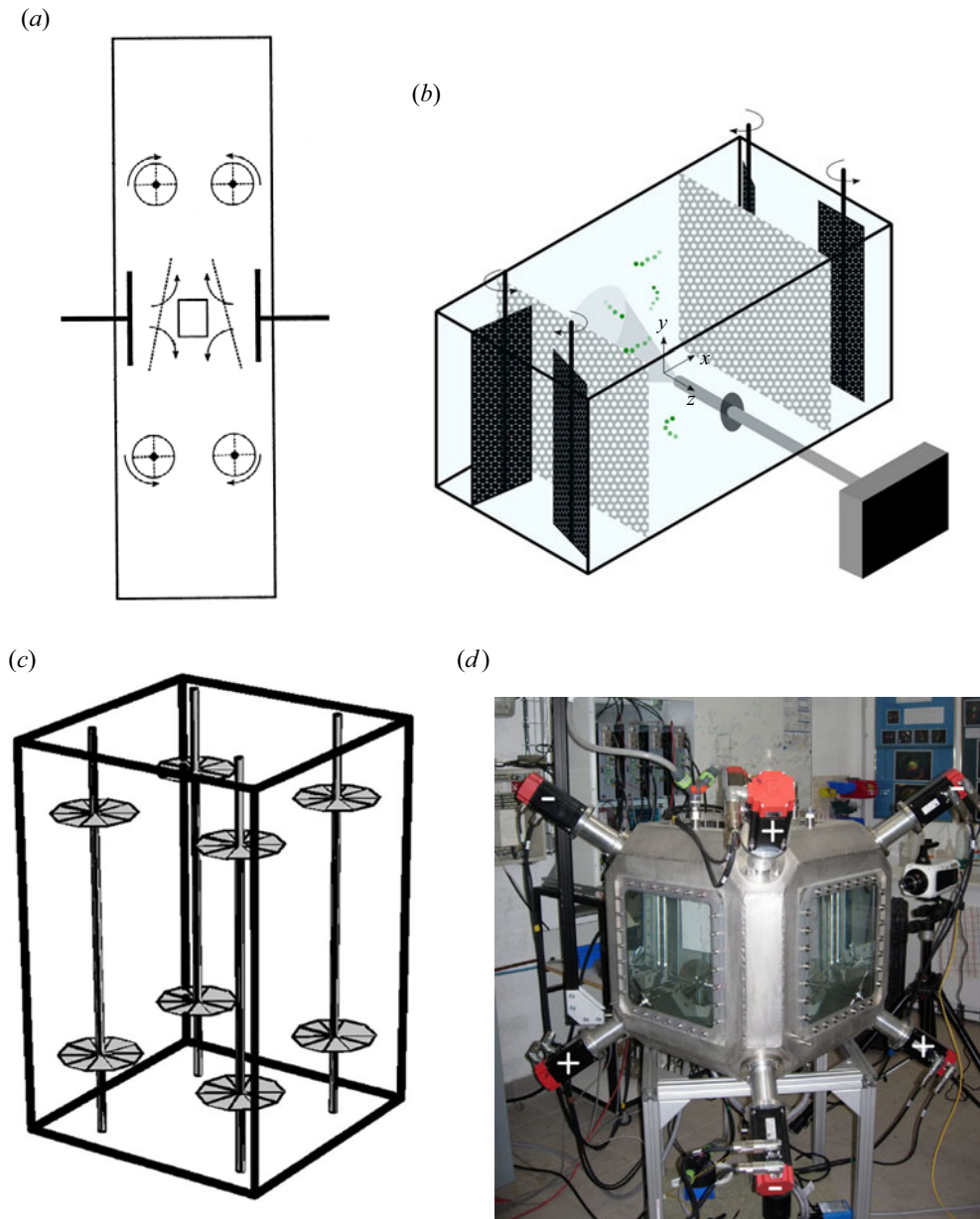
Figure 5. *Rotating element set-ups introduced in the experiments of (a) Liu et al. (1999), (b) Pujara et al. (2021), (c) Berg et al. (2006) and (d) Bounoua et al. (2018).*

3. Discussion

Using available data from the reviewed facilities, we summarize findings that suggest guiding principles for the generation of zero-mean-flow HIT. We first investigate the decay of turbulence in zero-mean-flow HIT facilities and draw comparisons with those with mean flow. We then consider the influence of forcing geometry on the generated HIT, and we subsequently explore non-dimensional relationships between forcing and the resulting turbulent scales across facilities.

3.1. Decay of turbulence

Physical mechanisms responsible for the decay of turbulence have been under debate for decades (de Karman & Howarth 1938; Batchelor & Townsend 1947; Frenkiel 1948). In turbulence-generating facilities, regions of the flow may experience a reduction in the strength of turbulence due to either increasing distance from the source (spatial decay) or unsteadiness in the driving mechanism (temporal decay). The variety of extant turbulence facilities provides an opportunity to investigate the dynamics of decay for different methods of forcing. While decay can be seen in integral scales, energy spectra, dissipation rate and many other flow metrics, we explore decay through the lens of turbulent kinetic energy. As the turbulence decays, the turbulent kinetic energy decreases, and other turbulence statistics respond accordingly.

In wind and water tunnels or flumes with upstream passive grid-generated turbulence (hereafter referred to as WWTs), spatial decay can be studied directly. Temporal decay can subsequently be determined by invoking Taylor's frozen turbulence hypothesis, given the mean velocity of the flow. In WWTs, k has been observed to decay as a power law with respect to time (or space) with a stage-dependent exponent of decay, n. This can be summarized by (3.1), in which x is a position downstream of virtual origin x_0 (de Karman & Howarth 1938; Kolmogorov 1941; Saffman 1967; Comte-Bellot & Corrsin 1971; Makita 1991):

$$k \sim (x - x_0)^{-n}. \tag{3.1}$$

In the first stage, the 'near-field' region, turbulence develops from the interaction of wakes from the passive or active grid. This region extends approximately $30\mathcal{L}_L$–$50\mathcal{L}_L$ beyond the grid (Krogstad & Davidson 2012). The second stage, the 'far-field' region, starts where HIT is developed. The value of n in both of these regions is highly dependent on the initial conditions and the initial Reynolds number (e.g. $n \approx [1.1$–$1.4]$ in the far field) (Valente & Vassilicos 2012; Thormann & Meneveau 2014). The final stage of decay, sometimes referred to as the 'tired turbulence' region (Batchelor 1953), where the dynamics of the flow is mainly affected by viscous rather than inertial forces, can be observed in sufficiently long tunnels assuming infinite boundaries. A general decay law with a single value of n can be applied to a broad range of studies for this region (Batchelor & Townsend 1948; Comte-Bellot & Corrsin 1966; Bennett & Corrsin 1978; George 1992; Touil, Bertoglio & Shao 2002; Biferale *et al.* 2003). The decay of the turbulence can be characterized as Saffman turbulence where $n \sim 3/2$ (Saffman 1967; Skrbek & Stalp 2000; Krogstad & Davidson 2010). However, before reaching this stage, $\mathcal{L}_L$ increases as k decays, leading to the confinement of large-scale motions by the smallest dimension of the domain. Consequently, these motions are of the same order of magnitude as the characteristic length scale and the turbulence decays at a higher rate (Skrbek & Stalp 2000).

Direct measurements of the velocity in zero-mean-flow HIT facilities enable the study of decay in different directions, which is beneficial when exploring how isotropy may vary in relation to decay. Both temporal and spatial decay can be observed directly from single-point, planar or volumetric velocity data. In facilities with planar forcing, spatial decay can be calculated as a function of distance from the source (e.g. Variano & Cowen 2008; Khorsandi *et al.* 2013; Pérez-Alvarado *et al.* 2016). Temporal decay can be measured directly by halting the forcing (i.e. turning off the actuators) (Hwang & Eaton 2004; Goepfert *et al.* 2010; Esteban *et al.* 2019). We can therefore compare various stages of decay between WWTs and zero-mean-flow HIT facilities.

In RJA facilities, the 'jet-merging' region is analogous to the near-field region of WWTs. In this region, energy from the mean flow of the individual jets transfers to the turbulent kinetic energy of the bulk HIT flow (Variano & Cowen 2008; Johnson & Cowen 2018). While the near-field region in WWTs is characterized by the exponential decay of k, we hypothesize that contrasting behaviour occurs in RJA-based facilities due to turbulence production from the time-varying jets; however, turbulence statistics have not explicitly been measured in this region of RJA-based or other zero-mean-flow HIT facilities. Thus, to estimate the length of the near-field region (or jet-merging region) in these facilities, we used the distance between the actuators and the reported HIT region. When normalizing this distance with

respect to $\mathcal{L}_L$, we observed that the near-field region is much smaller in RJA-based facilities than in WWTs, indicating that HIT forms more rapidly in RJA facilities due to the stochastic forcing. According to our analysis, beyond a distance from the array of $z_J/S > 6$, which is approximately equivalent to $6\mathcal{L}_L$–$10\mathcal{L}_L$ (where $\mathcal{L}_L$ is measured within the homogeneous and isotropic region), the zero-mean-flow HIT region is formed. In this far-field region, k decays with a power law in the forcing direction. The value of n reported for RJA facilities (e.g. Variano & Cowen 2008) was higher than those reported for WWTs. Variano & Cowen (2008) reported n to be approximately 2.3, which is closer to the values for the final stage of decay observed in WWTs. Similarly, in GST facilities, this value was reported to be approximately 2 (Hopfinger & Toly 1976).

Hwang & Eaton (2004) measured the temporal decay of the fluctuating velocities after turning off the actuators in a loudspeaker-driven facility with a spherical symmetric forcing system. The power-law decay exponent of the turbulent kinetic energy in this facility was $n = 1.86$, which is higher than the value estimated for the far field in WWT (Valente & Vassilicos 2012). During the decay, Hwang & Eaton (2004) found that the turbulence statistics were modified, yet remained isotropic. In a spherical symmetric forcing facility with no boundary, Goepfert et al. (2010) also studied temporal decay and found n to be approximately equal to 1.6. While n is somewhat facility-dependent, it is clear that the decay is faster in these two facilities than in the far-field region of WWT experiments; we hypothesize that this is also the case for zero-mean-flow HIT facilities in general.

Unlike Hwang & Eaton (2004) and Goepfert et al. (2010), who found a single value for n to characterize the temporal decay of k, Esteban et al. (2019) categorized multiple phases of decay based on different values of n. They found that immediately after turning off the jets, k decayed at a high rate, aligning well with the near-field region in WWT studies. Following this initial stage, the decay rate decreased and decelerated close to the range reported in the far-field region of WWTs. Esteban et al. (2019) continued the measurements further in time and found that the decay rate of k increased while the integral length scale remained constant. However, in the first two stages of decay, they observed a decrease in k accompanied by an increase in the integral length scale. They stated that the final phase of the observed temporal decay of the turbulence corresponds to the integral length scale being constrained by the facility size (i.e. indicating the saturation phase; Skrbek & Stalp 2000).

The decay rate in the final stage found by Esteban et al. (2019) is similar to the rates found by Hwang & Eaton (2004) and Goepfert et al. (2010), and it is higher than the decay rate in the far-field stage of WWT studies. Esteban et al. (2019) hypothesized that since the integral length scale in Hwang & Eaton (2004) was comparable to the size of the facility, their observed decay rate corresponded to the final saturation phase. By contrast, the lower decay rate reported by Goepfert et al. (2010) could be due to the absence of boundaries in their facility, thus precluding the presence of high velocity gradients (and concomitant energy dissipation) that develop close to a boundary. Analytical studies, such as Skrbek & Stalp (2000), suggest that in the region where $\mathcal{L}_L$ cannot grow further, due to confinement, k diminishes at an exponential decay rate of $n = 2$, which is similar to the values found in the aforementioned experimental studies (e.g. Hwang & Eaton 2004; Variano & Cowen 2008; Esteban et al. 2019). This is another indication that facility size strongly affects the integral length scale of the flow. As the Taylor-scale Reynolds number increases, $\mathcal{L}_L$ changes. However, the magnitude of $\mathcal{L}_L$ remains constrained by the size of the facility, as we discuss further in § 3.3.

Temporal decay can be directly measured in a zero-mean-flow facility and compared with decay in WWTs. However, if we consider comparing different stages of the spatial decay in WWTs and the zero-mean-flow HIT facilities, the spatial decay of turbulence does not have a counterpart in the far-field region of WWTs in terms of the decay exponent (as shown in figure 6). In addition to the absence of mean flow in these facilities (and thus the smaller distance needed to achieve HIT), we hypothesize that this is due to their different generation mechanisms and resulting flow dynamics. In WWTs, the very presence of mean flow drives production of shear and turbulence, and thus a longer distance is unavoidably necessary for the complete development of HIT. However, this is not the case in zero-mean-flow HIT facilities. According to the values of n presented for the spatial decay in HIT facilities (Esteban et al. 2019), turbulent length scales are likely to be affected by the confinement of the facility before

(*a*)

(*b*)
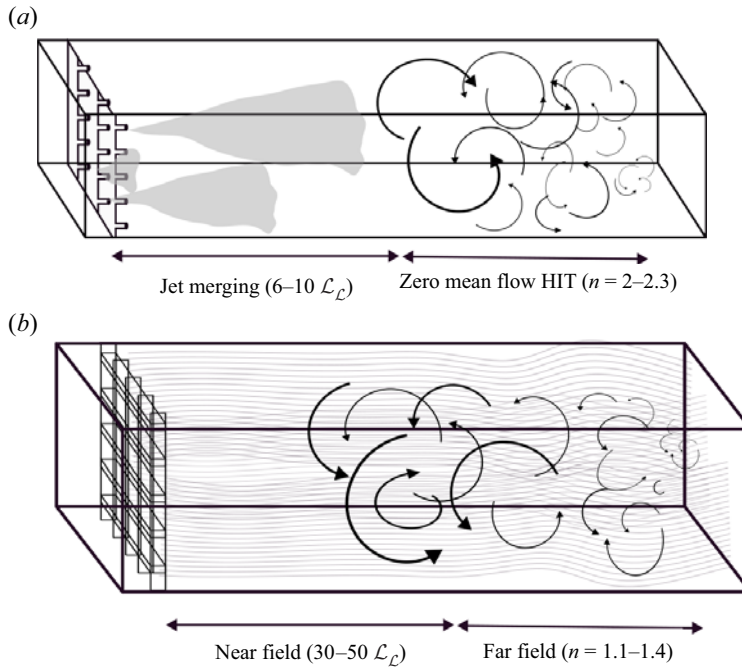
Figure 6. *Regions of decay in (a) RJA facility versus (b) WWTs. Distances are not to scale between (a) and (b) to enhance visualization.*

the far-field region develops. In most of the HIT studies presented here, the magnitude of the integral length scale is comparable to the size of the facility, consistent with the saturation phase. We propose that this is the reason faster decay rates (i.e. higher values of *n*) were observed as compared with in the far-field section of WWTs.

3.2. *Forcing geometry and physical aspects of facilities*

The spatial distribution of forcing elements affects the interaction of input momentum from individual actuators and can ultimately impact the resultant characteristics of the zero-mean-flow HIT region. Actuators may be directionally aligned in a closely spaced planar array (as in RJAs) or spaced widely, with generated flows oblique to one another (as in a spherical arrangement of loudspeakers). The forcing distribution may be categorized as symmetric or asymmetric. Symmetric forcing systems generate turbulence from multiple directions, resulting in a core volume of turbulence. Asymmetric forcing, with momentum input from a single direction, has been used to study mean-shear-free boundary layer dynamics or scalar transport at planar interfaces. Understanding the impact of the forcing distribution is crucial for optimizing the design of turbulence facilities and tailoring the resulting flow.

In asymmetrically forced facilities, where the source of input momentum is orthogonal to a single plane, it is reasonably assumed that the flow is radially symmetric in the plane perpendicular to the forcing direction at some distance downstream from the actuators (Variano & Cowen 2008; Johnson & Cowen 2018). In this type of forcing system, it is important to identify the location where the flow transitions from a region dominated by individual actuator activity to HIT with negligible mean flow (recall §§ 2.3 and 3.1). Several studies have explored the location of this transition (Variano & Cowen 2008; Masuk *et al.* 2019); however, further systematic investigation is needed.

In symmetric facilities, the HIT region is expected to be located at the centre of the facility. However, the size and shape of this region differ based on the type of actuator, the size of the facility, the forcing distribution and the forcing strength. For instance, spherical forcing systems (shown in figure 7*b*)
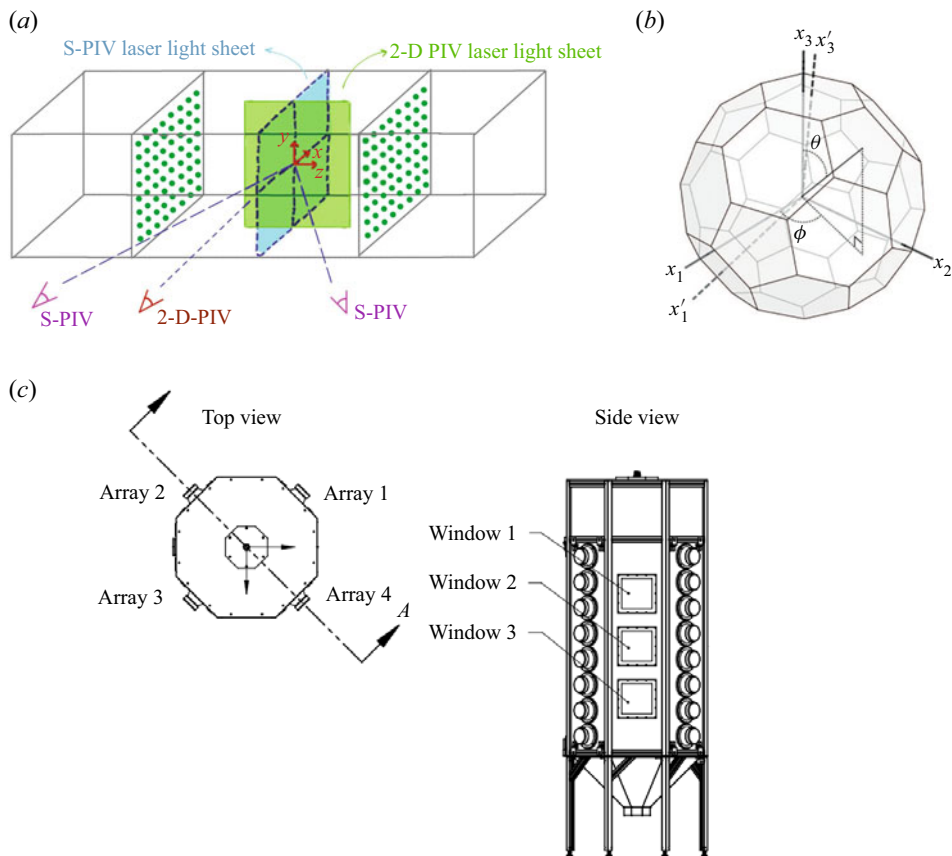
Figure 7. *Different types of symmetrically forced facilities. (a) Planar symmetric facility of* Bellani & Variano (2014), *(b) spherical symmetric facility of* Chang et al. (2012) *and (c) cylindrical symmetric facility of* Hoffman & Eaton (2021). *2-D, two-dimensional.*

generate spherical regions of HIT, while a cylindrical forcing system generates a long narrow turbulent region (the HIT region in the cylindrical facility of Hoffman & Eaton (2021) (figure 7c) had a high aspect ratio, with a height of $13\mathcal{L}_L$ and diameter of approximately $0.25\mathcal{L}_L$).

In systems with spherical forcing, achieving negligible mean flow may not require stochastic forcing. This is evident in the studies of Krawczynski *et al.* (2006, 2010), where turbulence produced with constant input forcing from all directions was not homogeneous, but a small region with negligible mean flow was identified. Interestingly, in the study of Chang *et al.* (2012), regions with higher values of k were associated with lower mean flow. We believe the resultant turbulence characteristics in these facilities are due to the interaction of input momentum from multiple opposing directions. This results in total reduction of mean flow and generation of turbulence with Ω close to 1.

Symmetric forcing may also be achieved using planar forcing with multiple actuator arrays, such as two or more facing RJAs, an example of which is shown in figure 7(a) (Bellani & Variano 2014; Carter *et al.* 2016; Bang & Pujara 2023). This forcing arrangement produces a cuboid-shaped zero-mean-flow HIT region that is widest in the plane perpendicular to the input forcing direction and narrowest in the direction of the input forcing (i.e. the depth of the HIT region). Multi-planar forcing systems can produce a larger HIT region compared with alternative symmetric forcing geometries. In these facilities, the depth of the HIT region, which is influenced by the decay of turbulence and the interaction of momentum-driven flows, is comparable to the size of the integral length scale of the turbulence (Bellani & Variano 2014). The height and width of the HIT region are constrained by the decay of

the fluctuating velocities due to the zero-energy condition at the boundaries (Bellani & Variano 2014; Johnson & Cowen 2018). We note that in several facilities, especially RJA-, fan- and loudspeaker-driven facilities, the homogeneous region has been shown to encompass multiple integral length scales, which can be useful for applications such as particle–turbulence interactions.

As previously discussed, flow behaviour and turbulence characteristics are strongly influenced by boundaries. This extends to all types of facilities and all boundaries (e.g. free surfaces, sediment beds, solid walls). Consequently, the influence of the boundaries on the flow statistics has been the focus of several theoretical, experimental and numerical studies (e.g. Thomas & Hancock 1977; Hunt & Graham 1978; Perot & Moin 1995). Many of the known laboratory-based zero-mean-shear boundary layer studies are performed in planar forcing facilities. For boundary planes perpendicular to the input forcing direction, turbulence metrics remain unaffected by the presence of boundaries at a distance greater than $1.5\mathcal{L}_L$ from the boundary (Delbos *et al.* 2009; Johnson & Cowen 2018). In addition, the effect of boundaries parallel to the input forcing extends $2\mathcal{L}_L$ into the facility (Variano & Cowen 2008; Bellani & Variano 2014). The type of boundary is also a crucial factor. Johnson & Cowen (2020) reveal significant differences in the boundary layer dynamics of turbulence metrics, such as fluctuating velocities and the integral length scale, depending on the type of the boundary (e.g. solid impermeable bed, flat sediment bed and rippled sediment bed).

In laboratory facilities, a distinct flow pattern may be established based on the momentum generated by the actuators and the characteristics of the boundaries, such as their position and type. The generated flow may develop into a large mean circulation or enhance standing waves with a specific frequency (i.e. loudspeakers; Sabban & van Hout 2011). One approach to reducing the likelihood of persistent mean circulations is to introduce spatial variability in the forcing pattern to interrupt the flow. Another technique is to induce temporal variability in the forcing mechanism, as discussed in § 1.1.3. For instance, in RJA facilities, the flow is constantly disturbed by jet flows generated by the pumps changing between on and off states, making it unlikely for large mean circulations to persist. While stochastic forcing generally reduces mean flows, a recent study with a planar impeller array found a peak in the temporal energy spectra (Lawson & Ganapathisubramani 2022), which was not observed in RJA facilities (Johnson & Cowen 2018), indicating that the rotational signature of impeller-type actuators may be challenging to eradicate in the resulting flow. It should be mentioned that even in RJA facilities with $M^* < 5\%$, tank-scale toroidal flows are often observed as bulk mean recirculations. Even though their contribution to the turbulence dynamics is negligible, these flows exist – both locally, to maintain conservation of mass immediately surrounding the actuators, and at the tank scale. Similarly, in loudspeaker-driven tanks, the frequency of the loudspeakers must be refined to avoid the generation of standing waves or recirculations of a certain mode in an enclosed facility. According to Goepfert *et al.* (2010), in facilities without boundaries, since the condition on mass flux is lifted, the forcing algorithm does not require variability to achieve negligible mean flow turbulence.

There are multiple approaches to change the turbulent flow characteristics once a facility is constructed. One is to add a mesh or perforated plate in front of the actuators (Hwang & Eaton 2004; Bellani *et al.* 2012; Carter *et al.* 2016; Pujara *et al.* 2021). Insertion of a mesh introduces smaller turbulence length scales by breaking up eddies into smaller sizes, altering the actuator-dominated flows and their interactions with the same input energy. For example, in RJA facilities with the same jet voltage, T_{on} and T_{off}, using a mesh immediately downstream of the pumps resulted in lower turbulent kinetic energy (Carter *et al.* 2016). Other modifications based on actuator type can be incorporated to further change the flow characteristics. In fan facilities, for example, changing the number of blades and/or pitch angle (recall § 2.1.1) can change flow metrics such as the turbulent Reynolds number and the integral length scale of the resultant HIT. We hypothesize that a higher number of blades leads to a reduction in $\mathcal{L}_L$ because the time for one blade's generated flow to be disturbed by the adjacent blade is shorter; therefore, the generated eddies are smaller in size, and the turbulent kinetic energy is lower.
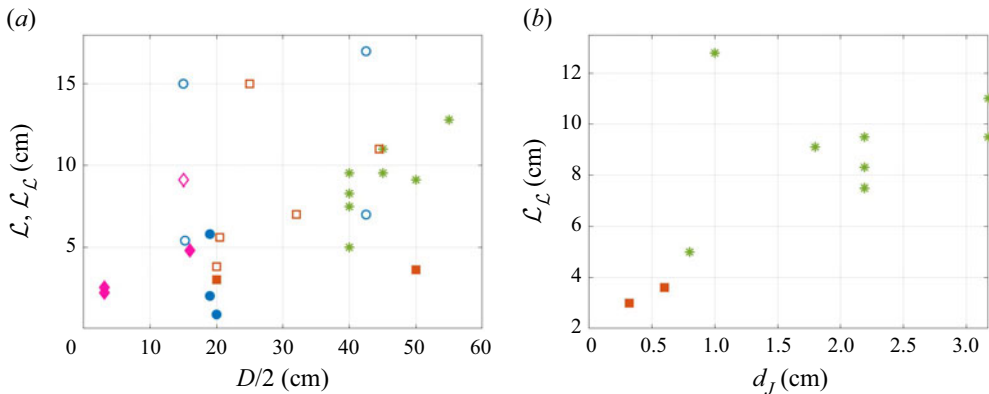
Figure 8. *Absolute (dimensional) variation of (a) large eddy length scale $\mathcal{L}$ and integral length scale $\mathcal{L}_L$ with facility half-width and (b) integral length scale with outlet jet diameter. The following markers represent facility type: loudspeakers ($\blacksquare$, red); RJAs ($*$, green); fans ($\bullet$, blue); and rotating elements ($\blacklozenge$, pink). The filled symbols represent $\mathcal{L}_L$ and the open symbols represent $\mathcal{L}$. See the Appendix (table 6) for full listing of sources from which data points were generated.*

3.3. Synthesis of forcing geometry and turbulence length scales across zero-mean-flow facilities

Previously, we discussed how physical aspects of a facility (forcing distribution, facility size, actuator characteristics, etc.) influence characteristics of the turbulence produced. In this section, we quantitatively investigate the extent of this influence. The importance of this topic is especially apparent in studies that employ the same flow-generation mechanism but with different overall size or forcing element spacing (e.g. Bellani & Variano 2014; Carter *et al.* 2016; Esteban *et al.* 2019). We use available data from many zero-mean-flow turbulence facilities (see the Appendix, table 6) to establish the relative importance of these variables.

Length scales inherent to a facility (i.e. overall facility size, actuator size and actuator spacing) can affect the resulting turbulent length scales. As discussed in § 3.1, it is likely that $\mathcal{L}_L$ is constrained by the size of the facility. Figure 8(*a*) reveals that larger facilities (as measured by $D/2$, the half-width of the smallest facility dimension) tend to have larger turbulent length scales. This is especially apparent when considering $\mathcal{L}_L$, more so than $\mathcal{L}$ (which is determined via scaling arguments when direct measurements of $\mathcal{L}_L$ are not available). Therefore, we focus our subsequent analysis on changes in $\mathcal{L}_L$ only; we note this precludes many facilities from the subsequent analysis due to a lack of data on these parameters, but we include as many facilities as possible to identify trends.

While $\mathcal{L}_L$ and $D/2$ are positively correlated, deviations from this correlation indicate the influence of other factors on the turbulent length scales. Additionally, some studies have reported different values of $\mathcal{L}_L$ in facilities with the same dimensions (e.g. Variano & Cowen 2008; Johnson & Cowen 2018), or observed changes in the value of $\mathcal{L}_L$ with varying input driving parameters (e.g. Carter *et al.* 2016; Johnson & Cowen 2018); this further supports the idea that other factors besides facility size can impact $\mathcal{L}_L$. Another physical length scale that can directly impact $\mathcal{L}_L$ is the outlet jet diameter, d_J. Parameter d_J is only relevant to RJAs and some of the loudspeaker-driven facilities with orifice plates. As is apparent in figure 8(*b*), there is a strong positive association between jet diameter and $\mathcal{L}_L$.

The equivalent actuator spacing, S_e, is a proposed counterpart to the mesh spacing in grid-generated turbulence (Hopfinger & Toly 1976; Kurian & Fransson 2009) and to actuator spacing in multi-jet array facilities (Yin, Zhang & Lin 2007; Berk, Gomit & Ganapathisubramani 2016). Parameter S_e describes a characteristic distance between active actuators, taking into account the stochasticity of spatial forcing in some facilities. It is equal to S in (non-stochastically forced) fan- and loudspeaker-driven facilities (see figure 9a), because all actuators are operating concurrently. In RJA facilities, since not all jets are activated simultaneously, S_e will be larger than the jet-to-jet spacing S (recall § 2.3). To define S_e in RJA

(*a*)   (*b*)
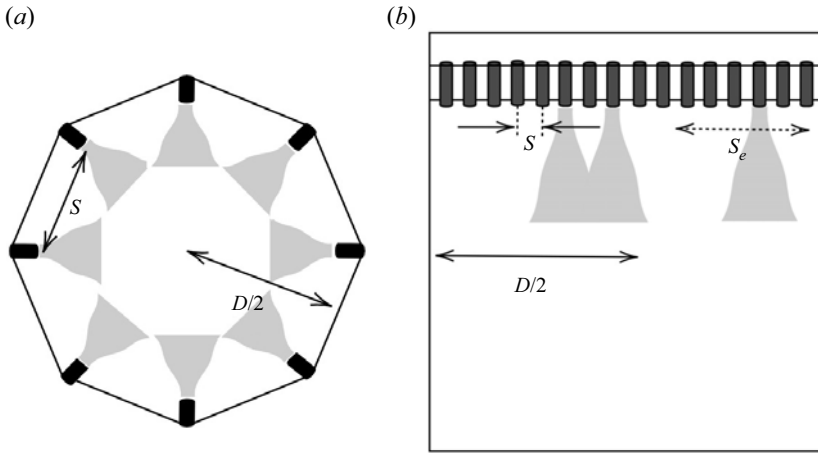
Figure 9. *Schematic diagrams of facilities with (a) symmetric vertex-mounted actuators and (b) planar actuator arrays indicating actuator spacing, equivalent actuator spacing and facility half-width.*
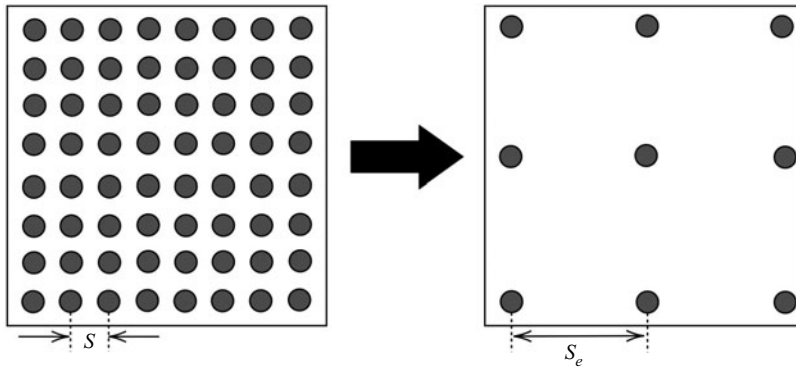
Figure 10. *Visualizations of jet spacing S (left) and equivalent actuator spacing S_e (right) for an 8×8 array of jets in an RJA facility with $\phi_{on} = 14\,\%$.*

facilities, we evenly distribute the number of jets that are, on average, operating at the same time across the overall area occupied by the original footprint of the jet array. The average number of jets operating simultaneously can be found by multiplying the total number of actuators, N, in an RJA facility by ϕ_{on}. These hypothetical 'active' actuators are then distributed across the original array footprint so as to maximize their spacing and ensure forcing across the entire facility, as shown in figure 10. We note that as ϕ_{on} decreases, S_e approaches facility size D, whereas as ϕ_{on} increases, S_e approaches geometric jet spacing S.

Figure 11(*a*) indicates that the integral length scale weakly increases with S_e (assuming $S_e = S$ for facilities with spatially uniform forcing). However, when we non-dimensionalize these two variables with respect to $D/2$ (figure 11*b*), this relationship disappears. This can be explained by the observation that, in general, as $D/2$ increases, S_e also increases. Non-dimensionalizing $\mathcal{L}_L$ with respect to $D/2$ removes its effect, resulting in no significant trends between S_e and $\mathcal{L}_L$. However, it is worth noting that in WWTs, there appears to be a positive correlation between the mesh spacing in grids and $\mathcal{L}_L$. Moreover, when non-dimensionalizing $\mathcal{L}_L$ with mesh spacing, the $\mathcal{L}_L$ values for different mesh spacings tend to collapse into a single curve (Kurian & Fransson 2009).

Another relevant scale is the ratio of the actuator diameter to equivalent actuator spacing, d_J/S_e, representing the length (or area, if squared) occupied by an outlet between two actuators. We note that
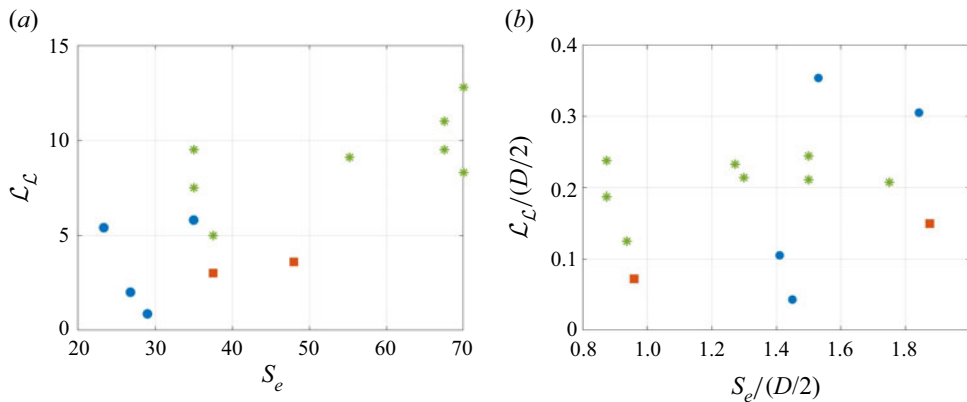
Figure 11. *Relationship between $\mathcal{L}_L$ and equivalent jet spacing S_e in (a) dimensional and (b) non-dimensional form. See figure 8(a) for legend.*
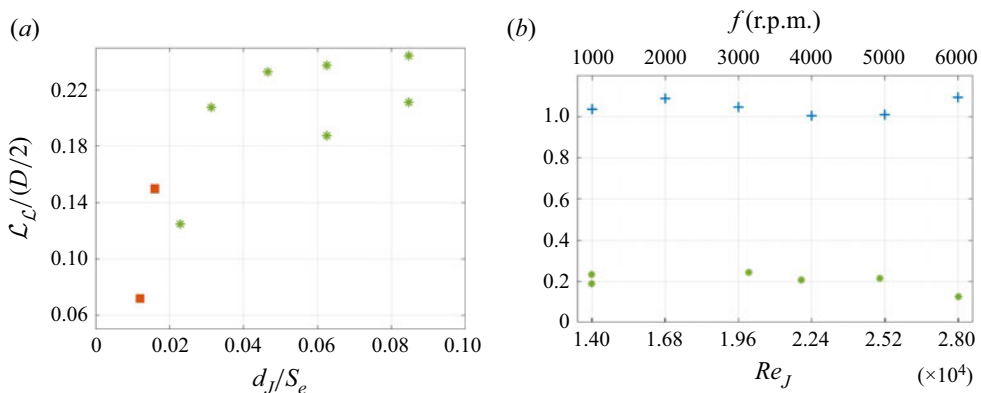
Figure 12. *Normalized integral length scale $\mathcal{L}_L/D/2$ versus (a) d_J/S_e (ratio of jet diameter to equivalent spacing) in RJA and loudspeaker-driven facilities and (b) outlet jet Reynolds number (lower axis) and fan rotational speed (Ravi et al. (2013), upper axis). Datapoints from Ravi et al. (2013) indicated with +. See figure 8(a) for legend of remaining markers.*

d_J/S_e is the inverse of the more commonly used non-dimensional jet spacing in many synthetic and non-synthetic jet studies (Greco *et al.* 2013; San & Chen 2014), which is known to influence characteristics of the generated turbulent flow. As shown in figure 12(*a*), a positive correlation exists between d_J/S_e and $\mathcal{L}_L$, indicating the possibility for higher values of $\mathcal{L}_L$ when the jet diameter occupies a larger proportion of the distance between actuators. It should be noted that we cannot imply that by simply increasing the number of active actuators (which would also decrease S_e), Re_λ will necessarily increase. Previous work with RJAs has explored the effect of increasing the mean percentage of active jets, and found an optimum of 12.5 % (Variano & Cowen 2008), indicating that the trend shown here is more intricate than solely changing d_J/S_e.

The outlet Reynolds number of the actuators, Re_J, is a crucial component of the interactions between the input momentum fluxes, and subsequently the generated HIT. Since d_J was shown to influence $\mathcal{L}_L$ (see figure 8*b*), it is plausible to assume that Re_J also affects $\mathcal{L}_L$. However, we find that the normalized integral length scale $\mathcal{L}_L$ does not vary with Re_J (figure 12*b*). This is consistent with findings from fan facilities, where $\mathcal{L}_L/D/2$ remains unchanged as fan rotational speed increases, as shown in figure 12(*b*) for a study by Ravi *et al.* (2013).
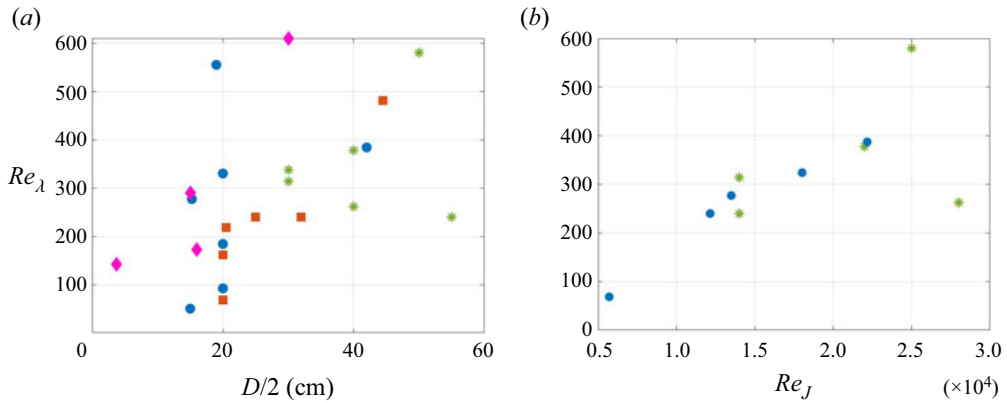
Figure 13. *The reported maximum Re_λ of generated turbulence with (a) facility length scale $D/2$ and (b) outlet Reynolds number for RJA and fan facilities. See figure 8(a) for legend.*

While Re_J does not directly affect $\mathcal{L}_L$ relative to facility size, it still plays an important role in other aspects of flow generation. For example, consider the ratio between the strength of the actuator outlet flux and the facility dimensions. If the flows generated by the actuators dissipate before interacting with each other, there will be no opportunity for HIT to form. This can occur if the actuators are not strong enough compared with the size of the facility. Conversely, if the actuators are spaced too closely, or if their outlet flow and input energy are too strong in relation to the available volume for HIT generation, the momentum may become amplified in particular directions, leading to higher levels of anisotropy (Chang *et al.* 2012; Carter *et al.* 2016; Esteban *et al.* 2019). From here we can discern a general governing principle for the design of turbulence-generating facilities: the size of the facility must be selected based on the ability of the actuator to impart sufficient momentum over a distance, which is a function of the actuator strength (Dou *et al.* 2016; Hoffman & Eaton 2021).

The ratio between Re_J and the available volume for turbulence generation can also affect the generation of total mean flow, especially when a negligible mean flow is desired. Small chambers often exhibit a smaller overall mean velocity compared with larger ones (Hwang & Eaton 2004; Hoffman & Eaton 2021). Additionally, Re_λ is typically lower in smaller facilities than in larger ones. Figure 13(a) shows that as the size of the facility increases, turbulent flow with higher Re_λ is generated. This may be due to the fact that achieving a high Re_λ requires high input axial momentum. We note that figure 13(a) includes only the maximum values of Re_λ reported for each facility. In small facilities, the limited space may impede momentum decay, resulting in a very high mean flow. Therefore, to maintain a negligible mean flow state, the input energy in the facility should be adjusted based on its size. For example, Rusello & Cowen (2015) (recall § 2.3) observed high values of mean flow strength due to high input energy relative to the size of the facility. Therefore, to produce zero-mean-flow HIT with desired characteristics, we speculate that higher values of Re_J are needed in larger facilities. This theory is supported by figure 13(b), which shows a positive relationship between Re_J and Re_λ. We note that for fan facilities, Re_J is calculated using the blade length or radius of the fan (whichever is available) as the length scale and fD_{fan} as the velocity scale.

As a final thought, we note that some facility designs may be more appropriate for certain investigative questions. For example, studies of decay may benefit from the use of actuators whose energy injection can be halted instantaneously. However, if the goal is to increase the overall energy injected into the flow, rotating elements may be more appropriate (recalling the previous discussion on how facility size may create a ceiling for Re_λ, and how injecting more energy may serve to increase mean flow up to the point where the flow cannot be assumed to have zero mean velocity). Those interested in Lagrangian turbulence or particle transport may wish to prioritize a design that maximizes the size of the homogeneous and isotropic region, due to the importance

of the history of the flow. Similar questions may also require greater tunability of the Kolmogorov length and time scales; however, we did not observe any consistent functional dependence of η or τ_η on the design parameters considered here. In all cases, facility designers should keep in mind the following major design parameters: (1) facility size and geometry, (2) actuator type, (3) actuator spacing/arrangement, (4) actuator energy level (e.g. Re_J or f) and (5) spatiotemporal variability in forcing. While there is no guaranteed formula for designing a turbulence facility with specific flow characteristics, the analysis provided within this section can provide a starting point.

4. Conclusions

Many innovative facilities have been designed to generate incompressible zero-mean-flow HIT; those presented herein all use some form of synthetic jets to induce momentum without adding net mass, with generation mechanisms (actuators) including fans, loudspeakers, RJAs and rotating elements. These facilities, which use different actuator types and arrangements, generate turbulence with varying flow properties. While the turbulence produced within each individual facility has been characterized to some degree, it is difficult to generalize across facilities to learn which design parameters are most influential and why. Here, we have provided a preliminary synthesis of the underlying relationships between facility design and resulting turbulence properties as a guide for future researchers when designing zero-mean-flow HIT facilities.

Actuator type (i.e. fans, loudspeakers, pumps, rotating elements) determines the characteristics of the input momentum flux, and subsequently the resulting turbulent flow. In fan-driven facilities, the effect of fan characteristics such as number of blades, blade length and rotational speed can affect turbulent kinetic energy and integral length scale. In loudspeaker-driven facilities, the signal that drives the loudspeakers and the properties of the loudspeakers (diameter of the loudspeaker and the characteristics of the orifice plate) are critical factors to turbulence generation. Similarly, in RJA facilities, the algorithm that drives the jets, the configuration of the jet arrays and physical characteristics of the jets are all important parameters that influence HIT formation. In addition to the actuator type, their positioning and forcing pattern can impact the produced HIT characteristics. Varying the distribution of forcing can generate unique turbulent environments. Symmetric forcing distributions (such as spherical, multi-planar and cylindrical symmetric forcing) versus asymmetric forcing distributions generate flows with different degrees of isotropy, decay rates and HIT region shapes and sizes.

For zero-mean-flow HIT facilities, the decay of turbulence plays a significant role, particularly in the direction of input forcing (for asymmetrically forced facilities). We used available data to investigate the decay of turbulence in these facilities and compared it with the decay patterns observed in wind and water tunnels. Notably, due to the absence of mean flow in the HIT facilities, the far-field region of WWTs does not have an equivalent counterpart in zero-mean-flow facilities. In general, the distance required from the actuators to reach a homogeneous and isotropic state was found to be smaller in zero-mean facilities compared with water and wind tunnels. Therefore, in the absence of mean flow, the development of HIT occurs more quickly and over a shorter duration.

Various physical length scales of the facilities contribute to characteristics of the developed HIT. Specifically, the integral length scale, $\mathcal{L}_L$, increases with an increase in $D/2$, d_J, S_e and d_J/S_e; surprisingly, $\mathcal{L}_L$ remains unchanged with Re_J. However, because larger facilities typically have larger actuator spacing, the correlation of $\mathcal{L}_L$ with S_e remains unclear, especially since the non-dimensional form of these parameters seems to be uncorrelated. Lack of a relationship between $\mathcal{L}_L$ and Re_J does not necessarily imply that the outlet flow of the actuators has no effect on the turbulence generated (e.g. Re_λ increases with Re_J), and other factors certainly play a role in determining $\mathcal{L}_L$. The relationships explored in § 3.3 are based on the reported average value of $\mathcal{L}_L$ in each study and thus show an overall trend rather than a strictly predictive relationship. Additionally, the relationship between the integral length scale and Re_J may not be linear, and thus a wider range of Re_J may need to be considered to fully investigate any potential correlation.

The dimensions of the facility and the strength of the momentum flux of the actuators are linked. To ensure the production of HIT with desired Re_λ and to prevent the occurrence of high mean flow, it is crucial to tune the features of the actuators in accordance with the facility size. If the input momentum flux is too strong or too weak compared with the facility size, the desired turbulence characteristics may not be achievable. Higher values of Re_λ can therefore be achieved in larger facilities by increasing Re_J, whereas increasing Re_J in smaller facilities could have other consequences.

Across the reviewed literature, there is not yet an established threshold for isotropy, though there are several approaches to evaluating flow properties via the ratios of turbulence parameters. The reported values of Ω_{ij} (evaluating isotropy of RMS velocities) across the included studies have some variation, but generally fall within the range of 1 ± 0.1 for facilities termed isotropic. Although it is challenging to define a precise cut-off point for isotropy, we propose that flows within this range ($0.9 < \Omega_{ij} < 1.1$) be considered isotropic, by virtue of consistency with existing facilities. This quantifiable and easily measured threshold provides a design goal for investigators seeking to create new facilities – one of the main objectives of this review. In certain experimental set-ups, the value of Ω_{ij} can also be adjusted by intentionally altering the forcing conditions, allowing for in-depth investigations into fundamental questions surrounding isotropic turbulence (e.g. Bewley *et al.* 2012; Chang *et al.* 2012; Carter & Coletti 2017).

The variability in the degree of isotropy and homogeneity, as well as the variety of HIT region sizes, Re_λ, turbulent length scales, strength of mean flow and other metrics considered here, indicates the uniqueness of each facility in the generation of turbulence as well as the need for generalizability and reproducibility. It also highlights the importance of selecting appropriate generation mechanisms and facility geometries to achieve desired turbulence characteristics. Computational simulations and laboratory techniques can be used to study the impact of different characteristics of facilities, which can lead to better understanding and manipulation of turbulent flows for a wide range of applications. The information provided herein can be used to optimally design turbulence facilities and determine control parameters for unique applications.

Declaration of interests. The authors declare no conflict of interest.

Author contributions. Data compilation, analysis, and interpretation were led by A.G.N. Manuscript writing was led by A.G.N. with supervision by B.A.J. and support from M.B. All authors provided valuable edits and input to the final draft.

A. Appendix

Table 6 summarizes technical specifications and flow characteristics of the HIT facilities presented above. The data are either presented directly from the original papers or are computed by the authors using information provided in the papers. We note that for each paper that presents a turbulence facility included in table 6, there may be subsequent papers that describe uses of the same facility for unique applications, possibly including modifications to the facility (e.g. changing Re_J, altering the working fluid, inserting mesh to reduce k) to do so. Application and modification papers are referenced throughout the paper, but are not included in this appendix.

Due to differences across studies regarding how data were measured, calculated or presented in their respective papers, we note the following considerations of the data presented herein:

(1) In some studies, the Taylor-scale Reynolds number was not available; therefore, other metrics are shown instead.

(2) The geometric shape of a facility can be determined by its dimensions. If only one value of L is presented, the geometry is cubic. If presented as three values of L, W and H, the geometry is

Table 6. *For caption see next page.*

Authors	Apparatus	Medium	u' (cm s^{-1})	w' (cm s^{-1})	$\langle U \rangle$ (cm s^{-1})	$\langle W \rangle$ (cm s^{-1})	Ω_{13}
Liu et al. (1999)	Rotating grids	Water	6	5.1	4.3	1.3	1.17$^{\times}$
Hwang & Eaton (2004)	Loudspeakers	Air	87	84	1.9	−8.8	1.03
Fallon & Rogers (2002)	Fans	Air	3	3	0.3	2	0.94
Birouk et al. (2003)	Fans	Air	25–90[3]	25–95[3]	−5–10[3]	−10–9[3]	0.9–1.1[3]
Webster et al. (2004)	Loudspeakers	Salt water	0.081–0.88	0.089–0.91	−0.07–0.07	−0.11–0.22	0.89–1.11
Berg et al. (2006)	Rotating disks	Water	2.2	1.5	—	—	1.47$^{\times}$
Variano & Cowen (2008)[4]	RJA	Water	3.91	4.98	0.26	0.10	0.78
de Jong et al. (2009)	Fans	Air	35.7–107	38–117	—	—	0.87–0.92$^{\times}$
Zimmermann et al. (2010)[6]	Fans	Water	1.5–12.6	—	0.1–1.1	—	—
Goepfert et al. (2010)	Loudspeakers	Air	83.5	87.7	3.3	−2.6	0.85–1.06
Sabban & van Hout (2011)	Loudspeakers	Air	48–58	52–64	−6–6	−1–3	0.94–0.92
Chang et al. (2012)[7]	Loudspeakers	Air	99	98	9.9	0.55	0.94
Ravi et al. (2013)[9]	Fans	Air	148	149	3	−1	0.99$^{\times}$
Khorsandi et al. (2013)[10]	RJA	Water	1.53	1.49	0.03	0.1	1.03
Carter et al. (2016)[11]	RJA	Air	38–76	—	—	—	1.37–1.72
Bellani & Variano (2014)[12]	RJA	Water	2.02	—	—	—	0.95
Pérez-Alvarado et al. (2016)[13]	RJA	Water	2.65	1.67	−0.01	−0.08	1.58
Dou et al. (2016)	Fans	Air	68–156	72–156	−4–9	−2–6	0.94–1.02$^{\times}$
Johnson & Cowen (2018)[14]	RJA	Water	4.08–5.19 4.61–5.97	5.53–7.01 5.68–7.78	—	—	0.72–0.74
Bradley et al. (2019)	Fans	Air	118–723	122–718	4–71	8–63	0.76–0.82$^{\times}$ 0.97–1.03$^{\times}$
Esteban et al. (2019)	RJA	Water	5.36	4.42	0.36	0.15	1.22$^{\times}$
Pujara et al. (2021)	Rotating grids	Water	0.7–1.87	0.8–3.23	0.036–0.061$^{\times}$	0.015–0.011$^{\times}$	0.875–0.579$^{\times}$
Hoffman & Eaton (2021)	Loudspeakers	Air	—	—	—	—	1–1.03

Table 6. *For caption see next page.*

Authors	$\dfrac{\langle U \rangle}{u'}$	Re_λ[1]	Re formula	M^* (%)	ϵ (m²s⁻³)	$\mathcal{L}, \mathcal{L}_L$ (cm)	η (μm)	Facility dimensions (cm)²
Liu et al. (1999)	0.71×	290	—	33.5×	2.3×10^{-3}	9.3*	140	$L=30$
Hwang & Eaton (2004)	0.022	220	$Re_\lambda = \dfrac{\lambda(k^2/12)^{1/2}}{\nu}$	0.3×	11	5.6*	130	$L=41$
Fallon & Rogers (2002)	0.1×	50	—	80×	—	15*	800	$L=30$
Birouk et al. (2003)	0.11–0.25×	45–92	$Re_\lambda = (15(\mathcal{L}/\eta)^{4/3})^{1/2}$	0.6–8×	—	0.86+	54–183	$L=40$
Webster et al. (2004)	0.08–0.86×	10–68	$Re_\lambda = \dfrac{u'\lambda}{\nu}$	86–2.28×	0.02–2.5×10^{-5}	3	450–1500	$L=40$
Berg et al. (2006)	—	172	$Re_\lambda = \dfrac{u'\lambda}{\nu}$	—	168×10^{-6}	4.8	250	$L=32,\ W=32,\ H=50$
Variano & Cowen (2008)[4]	0.07	314	$Re_\lambda = u'^2\sqrt{15/\nu\epsilon}$	1.05	5.2×10^{-4}	7.57+	210	$L=80,\ W=80,\ H=100$
de Jong et al. (2009)	—	104–184	$Re_\lambda = u'^2\sqrt{15/\nu\epsilon}$	—	1.51–38.7[5]	5.53–6.02*	97–217	$L=40$
Zimmermann et al. (2010)[6]	0.03–0.12×	150–330	$Re_\lambda = \dfrac{\lambda'_u}{\nu}$	0.1–1.5×	3.24×10^{-5} -3.6×10^{-2}	6–10*	73–420	$D=60$[8]
Goepfert et al. (2010)	0.039×	237	$Re_\lambda = \dfrac{\lambda(k^2/\bar{12})^{1/2}}{\nu}$	0.1×	6.7	3.6*	150	$L_S=68$
Sabban & van Hout (2011)	0.1–0.12×	144–162	$Re_\lambda = \dfrac{u'\lambda}{\nu}$	1.9–0.6×	2.4–3.99[5]	4.9–5.8×	172–195	$L=40$
Chang et al. (2012)[7]	0.04	481	$Re_\lambda = \dfrac{u'\lambda}{\nu}$	0.05×	6.7	—	155	$D=99$[8]
Ravi et al. (2013)[9]	0.02×	277	$Re_\lambda = \dfrac{u'\lambda}{\nu}$	0.02×	59.7	5.4*	100	$D=30.5,\ H=35.6$
Khorsandi et al. (2013)[10]	0.07	1800×	$Re_T = \dfrac{k^{1/2}\mathcal{L}}{\nu}$	1.13×	—	11+	—	$L=240,\ W=150,\ H=90$

Table 6. *Properties of turbulent flow generated in zero-mean-flow HIT facilities. Superscripts as explained in* table 2.

Authors	$\dfrac{\langle U\rangle}{u'}$	Re_λ^1	Re formula	M^* (%)	ϵ (m² s⁻³)	$\mathcal{L}, \mathcal{L}_L$ (cm)	η (μm)	Facility dimensions (cm)²
Carter et al. (2016)[11]	—	259–473	$Re_\lambda = \dfrac{u'\lambda}{\nu}$	—	0.1–1.2	9–14.6⁺	240–400	$L=110$, $W=200$, $H=240$
Bellani & Variano (2014)[12]	<0.10	338	$Re_\lambda = \dfrac{u'\lambda}{\nu}$	—	4.65×10^{-5}	9.5⁺	370	$L=80$, $W=80$, $H=360$
Pérez-Alvarado et al. (2016)[13]	0	2360	$Re_T = \dfrac{u'\mathcal{L}}{\nu}$	0.06×	—	11.5⁺	—	$L=240$, $W=150$, $H=90$
Dou et al. (2016)	0.02–0.07×	246–384	$Re_\lambda = \dfrac{u'\lambda}{\nu}$	0.2–0.3×	3.6–47	16–18*	100–179	$D=90^8$
Johnson & Cowen (2018)[14]	—	288–378 197–262	$Re_\lambda = u'^2\sqrt{15/\nu\epsilon}$	<5	$8.34\text{–}12.19\times 10^{-4}$ $20.17\text{–}35.93\times 10^{-4}$	6.8–9.71 4.63–5.19⁺	170–190 130–160	$L=80$, $W=80$, $H=100$
Bradley et al. (2019)	0.03–0.1×	220–555	$Re_\lambda = \dfrac{u'\lambda}{\nu}$	0.2–1×	—	1.91–2.15⁺	46–176	$D=38$
Esteban et al. (2019)	0.012	587	$Re_\lambda = \dfrac{u'\lambda}{\nu}$	0.2×	1.48×10^{-35}	9.1⁺	161	$L=240$, $W=85$, $H=100$
Pujara et al. (2021)	0.052–0.028	64–142	—	1.8–9.8	$6.9\text{–}160\times10^{-6}$	2.52–2.2⁺	280–620	$L=6.25$, $W=8.25$, $H=12.25$
Hoffman & Eaton (2021)	0.08–0.17	165–240	$Re_\lambda = \dfrac{(k^2/3)^{1/2}\lambda}{\nu}$	—	0.6–10.1	6.83–8.17*	135–269	$D=64$, $H=100$

cuboid. If presented as a single value of D, the object is assumed to be spherical, unless otherwise noted. However, if both D and H are listed, the object is cylindrical. Parameter L_S is defined in table 3.

(3) Values denoted here are estimated from figures presented in Birouk *et al.* (2003).

(4) The study of Variano & Cowen (2008) tested multiple algorithms; the results presented here are for the 'sunbathing' algorithm only.

(5) The studies of de Jong *et al.* (2009), Sabban & van Hout (2011) and Esteban *et al.* (2019) used multiple methods for calculating ϵ; the results presented here are only for the direct method. For the study of Esteban *et al.* (2019), the result presented uses the direct method with a correction factor applied.

(6) In the study of Zimmermann *et al.* (2010), u' is presented as the average of the RMS velocity measured in all three coordinate directions.

(7) The experiments of Chang *et al.* (2012) considered multiple isotropy ratios with the same Re_λ; here only the result for Ω closest to 1 is presented.

(8) The geometry of this facility is a truncated icosahedron.

(9) Multiple fan configurations have been tested. The result presented here is only for the base configuration.

(10) Results are presented for multiple locations; here only the result measured a distance $7.3S$ from the array is presented.

(11) Multiple set-up configurations were tested by Carter *et al.* (2016); only results for the baseline configuration are presented. In this study, u_T is presented instead of u'.

(12) The study of Bellani & Variano (2014) measured fluid velocity at several locations; here only the results from the tank centre are presented. In this study, u_T is presented instead of u'.

(13) The study of Pérez-Alvarado *et al.* (2016) measured fluid velocity at several locations with different jet-driving algorithms; only the results using the random algorithm at a distance $6.7S$ from the jet array are presented.

(14) In the study of Johnson & Cowen (2018), the first row presents data for the 8×8 RJA and the second row presents data for the 16×16 RJA.

References

ANDREWS, G., BRADLEY, D. & LWAKABAMBA, S. 1975 Measurement of turbulent burning velocity for large turbulent Reynolds numbers. *Symp. Combust.* **15** (1), 655–664.

ARONSON, D., JOHANSSON, A.V. & LÖFDAHL, L. 1997 Shear-free turbulence near a wall. *J. Fluid Mech.* **338**, 363–385.

BANG, J.Y. & PUJARA, N. 2023 Homogeneous turbulence in a random-jet-stirred tank. arXiv:2305.19430.

BATCHELOR, G.K. 1953 *The Theory of Homogeneous Turbulence*. Cambridge University Press.

BATCHELOR, G.K. & TOWNSEND, A. 1947 Decay of vorticity in isotropic turbulence. *Proc. R. Soc. Lond.* A **190** (1023), 534–550.

BATCHELOR, G.K. & TOWNSEND, A.A. 1948 Decay of turbulence in the final period. *Proc. R. Soc. Lond.* A **194** (1039), 527–543.

BELLANI, G., BYRON, M.L., COLLIGNON, A.G., MEYER, C.R. & VARIANO, E.A. 2012 Shape effects on turbulent modulation by large nearly neutrally buoyant particles. *J. Fluid Mech.* **712**, 41–60.

BELLANI, G. & VARIANO, E.A. 2014 Homogeneity and isotropy in a laboratory turbulent flow. *Exp. Fluids* **55** (1), 1646.

BENNETT, J.C. & CORRSIN, S. 1978 Small Reynolds number nearly isotropic turbulence in a straight duct and a contraction. *Phys. Fluids* **21** (12), 2129–2140.

BERG, J., LÜTHI, B., MANN, J. & OTT, S. 2006 Backwards and forwards relative dispersion in turbulent flow: an experimental investigation. *Phys. Rev.* E **74** (1), 016304.

BERK, T., GOMIT, G. & GANAPATHISUBRAMANI, B. 2016 Vectoring of parallel synthetic jets: a parametric study. *J. Fluid Mech.* **804**, 467–489.

BEWLEY, G.P., CHANG, K., BODENSCHATZ, E. & INTERNATIONAL COLLABORATION FOR TURBULENCE RESEARCH 2012 On integral length scales in anisotropic turbulence. *Phys. Fluids* **24** (6), 061702.

BEWLEY, G.P., SAW, E.-W. & BODENSCHATZ, E. 2013 Observation of the sling effect. *New J. Phys.* **15** (8), 083051.

BIFERALE, L., BOFFETTA, G., CELANI, A., LANOTTE, A., TOSCHI, F. & VERGASSOLA, M. 2003 The decay of homogeneous anisotropic turbulence. *Phys. Fluids* **15** (8), 2105–2112.

BIRINGEN, S. & REYNOLDS, W. 1981 Large-eddy simulation of the shear-free turbulent boundary layer. *J. Fluid Mech.* **103**, 53–63.

BIROUK, M., CHAUVEAU, C., SARH, B., QUILGARS, A. & GÖKALP, I. 1996 Turbulence effects on the vaporization of monocomponent single droplets. *Combust. Sci. Technol.* **113** (1), 413–428.

Birouk, M. & Gökalp, I. 2002 A new correlation for turbulent mass transfer from liquid droplets. *Intl J. Heat Mass Transfer* **45** (1), 37–45.

Birouk, M., Sarh, B. & Gökalp, I. 2003 An attempt to realize experimental isotropic turbulence at low Reynolds number. *Flow Turbul. Combust.* **70** (1–4), 325–348.

Blum, D.B., Kunwar, S.B., Johnson, J. & Voth, G.A. 2010 Effects of nonuniversal large scales on conditional structure functions in turbulence. *Phys. Fluids* **22** (1), 015107.

Bordoloi, A.D., Verhille, G. & Variano, E. 2019 Lagrangian time scale of rotation for inertial fibers in isotropic turbulence. arXiv:1910.02306.

Bounoua, S., Bouchet, G. & Verhille, G. 2018 Tumbling of inertial fibers in turbulence. *Phys. Rev. Lett.* **121** (12), 124502.

Bradley, D., Lawes, M. & Morsy, M.E. 2019 Measurement of turbulence characteristics in a large scale fan-stirred spherical vessel. *J. Turbul.* **20** (3), 195–213.

Brumley, B.H. & Jirka, G.H. 1987 Near-surface turbulence in a grid-stirred tank. *J. Fluid Mech.* **183**, 235–263.

Brunk, B. 1996 Modeling natural hydrodynamic systems with a differential-turbulence column. *J. Hydraul. Engng* **122** (7), 373–380.

Burattini, P., Antonia, R.A. & Danaila, L. 2005 Similarity in the far field of a turbulent round jet. *Phys. Fluids* **17** (2), 025101.

Byron, M., Einarsson, J., Gustavsson, K., Voth, G., Mehlig, B. & Variano, E. 2015 Shape-dependence of particle rotation in isotropic turbulence. *Phys. Fluids* **27** (3), 035101.

Carter, D., Petersen, A., Amili, O. & Coletti, F. 2016 Generating and controlling homogeneous air turbulence using random jet arrays. *Exp. Fluids* **57** (12), 189.

Carter, D.W. & Coletti, F. 2017 Scale-to-scale anisotropy in homogeneous turbulence. *J. Fluid Mech.* **827**, 250–284.

Carter, D.W. & Coletti, F. 2018 Small-scale structure and energy transfer in homogeneous turbulence. *J. Fluid Mech.* **854**, 505–543.

Casson, L.W. & Lawler, D.F. 1990 Flocculation in turbulent flow: measurement and modeling of particle size distributions. *J. Am. Water Works Assoc.* **82** (8), 54–68.

Chang, K., Bewley, G.P. & Bodenschatz, E. 2012 Experimental study of the influence of anisotropy on the inertial scales of turbulence. *J. Fluid Mech.* **692**, 464–481.

Comte-Bellot, G. & Corrsin, S. 1966 The use of a contraction to improve the isotropy of grid-generated turbulence. *J. Fluid Mech.* **25** (4), 657–682.

Comte-Bellot, G. & Corrsin, S. 1971 Simple Eulerian time correlation of full-and narrow-band velocity signals in grid-generated, 'isotropic' turbulence. *J. Fluid Mech.* **48** (2), 273–337.

Cromwell, T. 1960 Pycnoclines created by mixing in an aquarium tank. *J. Mar. Res.* **18**, 73–82.

Cuthbertson, A.J., Dong, P. & Davies, P.A. 2010 Non-equilibrium flocculation characteristics of fine-grained sediments in grid-generated turbulent flow. *Coast. Engng* **57** (4), 447–460.

Delbos, S., Weitbrecht, V., Bleninger, T., Grand, P.P., Chassaing, E., Lincot, D., Kerrec, O. & Jirka, G.H. 2009 Homogeneous turbulence at an electrodeposition surface induced by randomly firing jet arrays. *Exp. Fluids* **46** (6), 1105–1114.

DiBenedetto, M.H., Helfrich, K.R., Pires, A., Anderson, E.J. & Mullineaux, L.S. 2022 Responding to the signal and the noise: behavior of planktonic gastropod larvae in turbulence. *J. Expl Biol.* **225** (3), jeb243209.

Dickinson, S.C. & Long, R.R. 1983 Oscillating-grid turbulence including effects of rotation. *J. Fluid Mech.* **126**, 315–333.

Dohan, K. & Sutherland, B. 2002 Turbulence time scales in mixing box experiments. *Exp. Fluids* **33** (5), 709–719.

Doron, P., Bertuccioli, L., Katz, J. & Osborn, T.R. 2001 Turbulence characteristics and dissipation estimates in the coastal ocean bottom boundary layer from PIV data. *J. Phys. Oceanogr.* **31** (8), 2108–2134.

Dou, Z., Pecenak, Z.K., Cao, L., Woodward, S.H., Liang, Z. & Meng, H. 2016 PIV measurement of high-Reynolds-number homogeneous and isotropic turbulence in an enclosed flow apparatus with fan agitation. *Meas. Sci. Technol.* **27** (3), 035305.

Douady, S., Couder, Y. & Brachet, M.E. 1991 Direct observation of the intermittency of intense vorticity filaments in turbulence. *Phys. Rev. Lett.* **67** (8), 983–986.

Esteban, L.B., Shrimpton, J.S. & Ganapathisubramani, B. 2019 Laboratory experiments on the temporal decay of homogeneous anisotropic turbulence. *J. Fluid Mech.* **862**, 99–127.

Fallon, T. & Rogers, C. 2002 Turbulence-induced preferential concentration of solid particles in microgravity conditions. *Exp. Fluids* **33** (2), 233–241.

Fansler, T.D. & Groff, E.G. 1990 Turbulence characteristics of a fan-stirred combustion vessel. *Combust. Flame* **80** (3–4), 350–354.

Fauve, S., Laroche, C. & Castaing, B. 1993 Pressure fluctuations in swirling turbulent flows. *J. Phys. II* **3** (3), 271–278.

Fiabane, L., Volk, R., Pinton, J.-F., Monchaux, R., Cartellier, A. & Bourgoin, M. 2013 Do finite-size neutrally buoyant particles cluster? *Phys. Scr.* **2013** (T155), 014056.

Fiabane, L., Zimmermann, R., Volk, R., Pinton, J.-F. & Bourgoin, M. 2012 Clustering of finite-size particles in turbulence. *Phys. Rev. E* **86** (3), 035301.

Frenkiel, F. 1948 The decay of isotropic turbulence. *Trans. ASME J. Appl. Mech.* **15** (4), 311–321.

George, W.K. 1992 The decay of homogeneous isotropic turbulence. *Phys. Fluids* A **4** (7), 1492–1509.

Gibson, C. & Schwarz, W. 1963 The universal equilibrium spectra of turbulent velocity and scalar fields. *J. Fluid Mech.* **16** (3), 365–384.

GILLESPIE, L., LAWES, M., SHEPPARD, C. & WOOLLEY, R. 2000 Aspects of laminar and turbulent burning velocity relevant to SI engines. *SAE Trans*. **109**, 13–33.

GLEZER, A. & AMITAY, M. 2002 Synthetic Jets. *Annu. Rev. Fluid Mech*. **34** (1), 503–529.

GOEPFERT, C., MARIÉ, J.-L., CHAREYRON, D. & LANCE, M. 2010 Characterization of a system generating a homogeneous isotropic turbulence field by free synthetic jets. *Exp. Fluids* **48** (5), 809–822.

GORCE, J.-B. & FALCON, E. 2022 Statistical equilibrium of large scales in three-dimensional hydrodynamic turbulence. *Phys. Rev. Lett*. **129** (5), 054501.

GRECO, C.S., IANIRO, A., ASTARITA, T. & CARDONE, G. 2013 On the near field of single and twin circular synthetic air jets. *Intl J. Heat Fluid Flow* **44**, 41–52.

HOFFMAN, D.W. & EATON, J.K. 2021 Isotropic turbulence apparatus with a large vertical extent. *Exp. Fluids* **62** (10), 1–11.

HOLZNER, M., LIBERZON, A., GUALA, M., TSINOBER, A. & KINZELBACH, W. 2006 Generalized detection of a turbulent front generated by an oscillating grid. *Exp. Fluids* **41** (5), 711–719.

HOPFINGER, E.J. & TOLY, J.-A. 1976 Spatially decaying turbulence and its relation to mixing across density interfaces. *J. Fluid Mech*. **78** (1), 155–175.

HUNT, J.C.R. 1984 Turbulence structure in thermal convection and shear-free boundary layers. *J. Fluid Mech*. **138**, 161–184.

HUNT, J.C.R. & GRAHAM, J.M.R. 1978 Free-stream turbulence near plane boundaries. *J. Fluid Mech*. **84** (2), 209–235.

HWANG, W. & EATON, J. 2004 Creating homogeneous and isotropic turbulence without a mean flow. *Exp. Fluids* **36** (3), 444–454.

JIRKA, G.H., *et al.* 2008 Experiments on gas transfer at the air–water interface induced by oscillating grid turbulence. *J. Fluid Mech*. **594**, 183–208.

JOHNSON, B.A. & COWEN, E.A. 2018 Turbulent boundary layers absent mean shear. *J. Fluid Mech*. **835**, 217–251.

JOHNSON, B.A. & COWEN, E.A. 2020 Sediment suspension and bed morphology in a mean shear free turbulent boundary layer. *J. Fluid Mech*. **894**, A8.

DE JONG, J., CAO, L., WOODWARD, S.H., SALAZAR, J.P.L.C., COLLINS, L.R. & MENG, H. 2009 Dissipation rate estimation from PIV in zero-mean isotropic turbulence. *Exp. Fluids* **46** (3), 499–515.

DE KARMAN, T. & HOWARTH, L. 1938 On the statistical theory of isotropic turbulence. *Proc. R. Soc. Lond*. A **164** (917), 192–215.

KHORSANDI, B., GASKIN, S. & MYDLARSKI, L. 2013 Effect of background turbulence on an axisymmetric turbulent jet. *J. Fluid Mech*. **736**, 250–286.

KIT, E.L.G., STRANG, E.J. & FERNANDO, H.J.S. 1997 Measurement of turbulence near shear-free density interfaces. *J. Fluid Mech*. **334**, 293–314.

KLEIN, S., GIBERT, M., BÉRUT, A. & BODENSCHATZ, E. 2012 Simultaneous 3D measurement of the translation and rotation of finite-size particles and the flow field in a fully developed turbulent water flow. *Meas. Sci. Technol*. **24** (2), 024006.

KOLMOGOROV, A.N. 1941 The local structure of turbulence in incompressible viscous fluid for very large Reynolds numbers. *C. R. Acad. Sci*. **434** (1890), 301–305.

KRAWCZYNSKI, J.F., RENOU, B. & DANAILA, L. 2010 The structure of the velocity field in a confined flow driven by an array of opposed jets. *Phys. Fluids* **22** (4), 045104.

KRAWCZYNSKI, J.F., RENOU, B., DANAILA, L. & DEMOULIN, F.X. 2006 Small-scale measurements in a partially stirred reactor. *Exp. Fluids* **40** (5), 667–682.

KROGSTAD, P.-Å. & DAVIDSON, P. 2010 Is grid turbulence saffman turbulence? *J. Fluid Mech*. **642**, 373–394.

KROGSTAD, P.-Å. & DAVIDSON, P.A. 2012 Near-field investigation of turbulence produced by multi-scale grids. *Phys. Fluids* **24** (3), 035103.

KUMARESAN, T. & JOSHI, J.B. 2006 Effect of impeller design on the flow pattern and mixing in stirred tanks. *Chem. Engng J*. **115** (3), 173–193.

KURIAN, T. & FRANSSON, J.H. 2009 Grid-generated turbulence revisited. *Fluid Dyn. Res*. **41** (2), 021403.

KWON, S., WU, M.-S., DRISCOLL, J. & FAETH, G. 1992 Flame surface properties of premixed flames in isotropic turbulence: measurements and numerical simulations. *Combust. Flame* **88** (2), 221–238.

LAVERTU, T.M. 2006 Differential diffusion in a turbulent jet. PhD thesis, McGill University.

LAWSON, J.M., BODENSCHATZ, E., KNUTSEN, A.N., DAWSON, J.R. & WORTH, N.A. 2019 Direct assessment of Kolmogorov's first refined similarity hypothesis. *Phys. Rev. Fluids* **4** (2), 022601.

LAWSON, J.M. & GANAPATHISUBRAMANI, B. 2022 Unsteady forcing of turbulence by a randomly actuated impeller array. *Exp. Fluids* **63** (1), 13.

LEISENHEIMER, B. & LEUCKEL, W. 1996 Self-generated acceleration of confined deflagrative flame fronts. *Combust. Sci. Technol*. **118** (1–3), 147–164.

LI, M., LOHSE, D. & HUISMAN, S.G. 2023 High humidity enhances the evaporation of non-aqueous volatile sprays. *J. Fluid Mech*. **956**, A19.

LI, W., ZHANG, P., YANG, S., FU, X. & XIAO, Y. 2020 An experimental method for generating shear-free turbulence using horizontal oscillating grids. *Water* **12** (2), 591.

LIU, S., KATZ, J. & MENEVEAU, C. 1999 Evolution and modelling of subgrid scales during rapid straining of turbulence. *J. Fluid Mech*. **387**, 281–320.

LU, J., FUGAL, J.P., NORDSIEK, H., SAW, E.W., SHAW, R.A. & YANG, W. 2008 Lagrangian particle tracking in three dimensions via single-camera in-line digital holography. *New J. Phys*. **10** (12), 125013.

MAKITA, H. 1991 Realization of a large-scale turbulence field in a small wind tunnel. *Fluid Dyn. Res*. **8** (1–4), 53–64.

Mann, J., Ott, S. & Andersen, J.S. 1999 *Experimental Study of Relative, Turbulent Diffusion*. Technical University of Denmark.

Marston, J. & Tobias, S. 2022 Recent developments in theories of inhomogeneous and anisotropic turbulence. *Annu. Rev. Fluid Mech.* **55**, 351–375.

Masuk, A.U.M., Salibindla, A., Tan, S. & Ni, R. 2019 V-ONSET (Vertical Octagonal Noncorrosive Stirred Energetic Turbulence): a vertical water tunnel with a large energy dissipation rate to study bubble/droplet deformation and breakup in strong turbulence. *Rev. Sci. Instrum.* **90** (8), 085105.

Matsuzawa, T., Mitchell, N.P., Perrard, S. & Irvine, W.T. 2023 Creation of an isolated turbulent blob fed by vortex rings. *Nat. Phys.* **19**, 1–8.

McCorquodale, M.W. & Munro, R. 2018 A method for reducing mean flow in oscillating-grid turbulence. *Exp. Fluids* **59** (12), 182.

McCutchan, A. 2020 The development of an experimental apparatus to investigate ice melting rates via homogeneous isotropic turbulence. Master's project, The University of Texas at Austin.

McCutchan, L.A. & Johnson, A.B. 2023 An experimental apparatus for generating homogeneous isotropic turbulence. *Exp. Fluids* **64** (11), 177.

McDougall, T.J. 1979 Measurements of turbulence in a zero-mean-shear mixed layer. *J. Fluid Mech.* **94** (3), 409–431.

Mcgrath, J.L., Fernando, H.J.S. & Hunt, J.C.R. 1997 Turbulence, waves and mixing at shear-free density interfaces. Part 2. Laboratory experiments. *J. Fluid Mech.* **347**, 235–261.

McKenna, S.P. & McGillis, W.R. 2004 Observations of flow repeatability and secondary circulation in an oscillating grid-stirred tank. *Phys. Fluids* **16** (9), 3499–3502.

Medina, P., Sánchez, M. & Redondo, J. 2001 Grid stirred turbulence: applications to the initiation of sediment motion and lift-off studies. *Phys. Chem. Earth* B **26** (4), 299–304.

Meyer, C.R., Byron, M.L. & Variano, E.A. 2013 Rotational diffusion of particles in turbulence: rotational diffusion of particles in turbulence. *Limnol. Oceanogr.* **3** (1), 89–102.

Mydlarski, L. 2017 A turbulent quarter century of active grids: from Makita (1991) to the present. *Fluid Dyn. Res.* **49** (6), 061401.

Ni, R., Kramel, S., Ouellette, N.T. & Voth, G.A. 2015 Measurements of the coupling between the tumbling of rods and the velocity gradient tensor in turbulence. *J. Fluid Mech.* **766**, 202–225.

Nokes, R. 1988 On the entrainment rate across a density interface. *J. Fluid Mech.* **188**, 185–204.

Oehmke, T.B. & Variano, E.A. 2021 A new particle for measuring mass transfer in turbulence. *Exp. Fluids* **62** (1), 16.

Orlins, J. & Gulliver, J.S. 2003 Turbulence quantification and sediment resuspension in an oscillating grid chamber. *Exp. Fluids* **34** (6), 662–677.

Ouellette, N.T., Xu, H., Bourgoin, M. & Bodenschatz, E. 2006 Small-scale anisotropy in Lagrangian turbulence. *New J. Phys.* **8** (6), 102.

Pérez-Alvarado, A., Mydlarski, L. & Gaskin, S. 2016 Effect of the driving algorithm on the turbulence generated by a random jet array. *Exp. Fluids* **57** (2), 20.

Perot, B. & Moin, P. 1995 Shear-free turbulent boundary layers. Part 1. Physical insights into near-wall turbulence. *J. Fluid Mech.* **295**, 199–227.

Petersen, A.J., Baker, L. & Coletti, F. 2019 Experimental study of inertial particles clustering and settling in homogeneous turbulence. *J. Fluid Mech.* **864**, 925–970.

Pope, S.B. 2000 *Turbulent Flows*. Cambridge University Press.

Pratt, K.R., True, A. & Crimaldi, J.P. 2017 Turbulent clustering of initially well-mixed buoyant particles on a free-surface by Lagrangian coherent structures. *Phys. Fluids* **29** (7), 075101.

Pujara, N., Clos, K.T.Du, Ayres, S., Variano, E.A. & Karp-Boss, L. 2021 Measurements of trajectories and spatial distributions of diatoms (Coscinodiscus spp.) at dissipation scales of turbulence. *Exp. Fluids* **62** (7), 149.

Pujara, N., Oehmke, T.B., Bordoloi, A.D. & Variano, E.A. 2018 Rotations of large inertial cubes, cuboids, cones, and cylinders in turbulence. *Phys. Rev. Fluids* **3** (5), 054605.

Pujol, D., Colomer, J., Serra, T. & Casamitjana, X. 2010 Effect of submerged aquatic vegetation on turbulence induced by an oscillating grid. *Cont. Shelf Res.* **30** (9), 1019–1029.

Ravi, S., Peltier, S.J. & Petersen, E.L. 2013 Analysis of the impact of impeller geometry on the turbulent statistics inside a fan-stirred, cylindrical flame speed vessel using PIV. *Exp. Fluids* **54** (1), 1424.

Rouse, H. & Dodu, G. 1955 Turbulent diffusion across a density discontinuity. *La Houille Blanche* **10**, 530–532.

Rusello, P.J. & Cowen, E.A. 2015 Design and characterization of a turbulence chamber for scalar flux measurements at a sediment-water interface. *J. Environ. Engng* **141** (3), 04014062.

Sabban, L., Cohen, A. & van Hout, R. 2017 Temporally resolved measurements of heavy, rigid fibre translation and rotation in nearly homogeneous isotropic turbulence. *J. Fluid Mech.* **814**, 42–68.

Sabban, L. & van Hout, R. 2011 Measurements of pollen grain dispersal in still air and stationary, near homogeneous, isotropic turbulence. *J. Aerosol. Sci.* **42** (12), 867–882.

Saffman, P.G. 1967 Note on Decay of Homogeneous Turbulence. *Phys. Fluids* **10** (6), 1349.

Salazar, J.P., Jong, J.De, Cao, L., Woodward, S.H., Meng, H. & Collins, L.R. 2008 Experimental and numerical investigation of inertial particle clustering in isotropic turbulence. *J. Fluid Mech.* **600**, 245–256.

San, J.-Y. & Chen, J.-J. 2014 Effects of jet-to-jet spacing and jet height on heat transfer characteristics of an impinging jet array. *Intl J. Heat Mass Transfer* **71**, 8–17.

Semenov, E.S. 1965 Measurement of turbulence characteristics in a closed volume with artificial turbulence. *Combust. Explos. Shock Waves* **1** (2), 57–62.

Shy, S., Jang, R. & Tang, C. 1996 Simulation of turbulent burning velocities using aqueous autocatalytic reactions in a near-homogeneous turbulence. *Combust. Flame* **105** (1–2), 54–67.

Shy, S., Tang, C. & Fann, S. 1997 A nearly isotropic turbulence generated by a pair of vibrating grids. *Exp. Therm. Fluid Sci*. **14** (3), 251–262.

Simmons, L. & Salter, C. 1934 Experimental investigation and analysis of the velocity variations in turbulent flow. *Proc. R. Soc. Lond*. A **145** (854), 212–234.

Skrbek, L. & Stalp, S.R. 2000 On the decay of homogeneous isotropic turbulence. *Phys. Fluids* **12** (8), 1997–2019.

Smith, B.L. & Glezer, A. 1998 The formation and evolution of synthetic jets. *Phys. Fluids* **10** (9), 2281–2297.

Srdic, A., Fernando, H. & Montenegro, L. 1996 Generation of nearly isotropic turbulence using two oscillating grids. *Exp. Fluids* **20** (5), 395–397.

Sreenivasan, K.R. 1984 On the scaling of the turbulence energy dissipation rate. *Phys. Fluids* **27** (5), 1048–1051.

Stapountzis, H., Dimitriadis, T.-G., Giourgas, K. & Kotsanidis, K. 2015 Melting of ice spheres in nearly isotropic turbulence with zero mean. In *Proceedings of the 10th Pacific Symposium on Flow Visualization and Image Processing*, pp. 15–18.

Tennekes, H. & Lumley, J.L. 1972 *A First Course in Turbulence*. MIT Press.

Thomas, N. & Hancock, P. 1977 Grid turbulence near a moving wall. *J. Fluid Mech*. **82** (3), 481–496.

Thompson, S. & Turner, J. 1975 Mixing across an interface due to turbulence generated by an oscillating grid. *J. Fluid Mech*. **67** (2), 349–368.

Thormann, A. & Meneveau, C. 2014 Decay of homogeneous, nearly isotropic turbulence behind active fractal grids. *Phys. Fluids* **26** (2), 025112.

Tinklenberg, A., Guala, M. & Coletti, F. 2023 Thin disks falling in air. *J. Fluid Mech*. **962**, A3.

Toschi, F. & Bodenschatz, E. 2009 Lagrangian properties of particles in turbulence. *Annu. Rev. Fluid Mech*. **41**, 375–404.

Touil, H., Bertoglio, J.-P. & Shao, L. 2002 The decay of turbulence in a bounded domain. *J. Turbul*. **3**, N49.

Tsai, C.-H. & Lick, W. 1986 A portable device for measuring sediment resuspension. *J. Great Lakes Res*. **12** (4), 314–321.

Uzkan, T. & Reynolds, W. 1967 A shear-free turbulent boundary layer. *J. Fluid Mech*. **28** (4), 803–821.

Valente, P. & Vassilicos, J. 2012 Dependence of decaying homogeneous isotropic turbulence on inflow conditions. *Phys. Lett*. A **376** (4), 510–514.

Variano, E.A., Bodenschatz, E. & Cowen, E.A. 2004 A random synthetic jet array driven turbulence tank. *Exp. Fluids* **37** (4), 613–615.

Variano, E.A. & Cowen, E.A. 2008 A random-jet-stirred turbulence tank. *J. Fluid Mech*. **604**, 1–32.

Villermaux, E., Sixou, B. & Gagne, Y. 1995 Intense vortical structures in grid-generated turbulence. *Phys. Fluids* **7** (8), 2008–2013.

Voth, G.A., Porta, A.La, Crawford, A.M., Alexander, J. & Bodenschatz, E. 2002 Measurement of particle accelerations in fully developed turbulence. *J. Fluid Mech*. **469**, 121–160.

Walker, D., Leighton, R. & Garza-Rios, L.O. 1996 Shear-free turbulence near a flat free surface. *J. Fluid Mech*. **320**, 19–51.

Webster, D. & Young, D. 2015 A laboratory realization of the burgers' vortex cartoon of turbulence-plankton interactions. *Limnol. Oceanogr*. **13** (2), 92–102.

Webster, D.R., Brathwaite, A. & Yen, J. 2004 A novel laboratory apparatus for simulating isotropic oceanic turbulence at low Reynolds number. *Limnol. Oceanogr*. **2** (1), 1–12.

Xu, S., Huang, S., Huang, R., Wei, W., Cheng, X., Ma, Y. & Zhang, Y. 2017 Estimation of turbulence characteristics from PIV in a high-pressure fan-stirred constant volume combustion chamber. *Appl. Therm. Engng* **110**, 346–355.

Xuequan, E. & Hopfinger, E.J. 1986 On mixing across an interface in stably stratified fluid. *J. Fluid Mech*. **166**, 277–244.

Yang, T. & Shy, S. 2003 The settling velocity of heavy particles in an aqueous near-isotropic turbulence. *Phys. Fluids* **15** (4), 868–880.

Ye, L., Manning, A.J. & Hsu, T.-J. 2020 Oil-mineral flocculation and settling velocity in saline water. *Water Res*. **173**, 115569.

Yin, Z.-Q., Zhang, H.-J. & Lin, J.-Z. 2007 Experimental study on the flow field characteristics in the mixing region of twin jets. *J. Hydrodyn*. **19** (3), 309–313.

Zellouf, Y., Dupont, P. & Peerhossaini, H. 2005 Heat and mass fluxes across density interfaces in a grid-generated turbulence. *Intl J. Heat Mass Transfer* **48** (18), 3722–3735.

Zhou, Y. 2021 Turbulence theories and statistical closure approaches. *Phys. Rep*. **935**, 1–117.

Zimmermann, R., Xu, H., Gasteuil, Y., Bourgoin, M., Volk, R., Pinton, J.-F., Bodenschatz, E. & Research, I.C.F.T. 2010 The Lagrangian exploration module: an apparatus for the study of statistically homogeneous and isotropic turbulence. *Rev. Sci. Instrum*. **81** (5), 055112.